SMART STRUCTURES ANALISYS

APPLICATION TO SANDWICH STRUCTURES

Author:
Alberto Sisamón Serrano

Director of research:
Enrique Barbero Pozuelo

Leganés, September 2015

To mum, dad and brother. Thank you.

"Art without engineering is dreaming.
Engineering without art is calculating."

Steven Roberts

Abstract

Control of the surface shape is one of the most interesting applications of smart materials into morphing structures. This Undergraduate Thesis Project aims the determination of the smart materials capabilities to control beam deformations. Different analyses are performed to a sandwich beam with piezoelectric materials embedded within it in order to quantify the contribution to the beam deflections of the response of the piezoelectric actuators to the presence of an electric field in the environment. The temperature difference existing in the beam surroundings is also studied to analyze if it affects the piezoelectric capability to modify the beam response. The analytic model for predicting beam deformations, accounting with the contribution of the piezoelectric actuator is based on the Kirchhoff beam model, combined with the Classical Laminated Plate Theory for composite laminae behavior description applied to sandwich beams.

Contents

List of Figures

List of Tables

CHAPTER 1

Introduction

1.1 Motivation

The development of smart structures has enabled a change in the structural design concept. Earlier, traditional structural design was conceived to be restricted to the optimum material selection and the correct dimensioning to guarantee that the structure is able to withstand the forecast loads expected during its lifetime. Now, this traditional structural design is changing since it can consider the design of structures which can adapt to the environment and monitor its status with the chance to be repaired by themselves.

Smart structures are any *system or material which has built-in or intrinsic sensors, actuators and control mechanisms whereby it is capable of sensing a stimulus, responding to it in a predetermined manner and extent, in a short appropriate time, and reverting to its original state as soon as the stimulus is removed*, according to the definition of Ahmad[1] adopted in the workshop organized by the US Army Research Office in 1988. Smart materials were born following a constant evolution in the engineering and material sciences: starting from the use of inert and basic materials, following by more and more sophisticated materials with higher strength and lower weight built for a particular function, and arriving to smart materials, adaptive material specimens with reaction capabilities.

Smart structures are capable of monitoring and responding to changes in the surrounding environment. The monitoring function is directed towards improving safety and maintenance scheduling. The response function deals with the possibility of controlling the elasto-mechanical properties of the structure such as shape, stiffness or vibration, producing higher performance and reduction in weight [2].

The control and reaction capabilities of smart structures can entail important implications in their application on the industry. The response function can be used to reduce vibrations and noise or stress at which the structure is subjected by reacting against the environment stimuli through the actuators mechanisms. These structure reactions will imply an increase of the structure's lifetime. It is also applied for the modification of the shape of the structure to optimum one

defined by the operating conditions, increasing the structure performance. The control capability can be used in structures such as buildings, ships or aircraft, where a confident designed and a regular inspection is needed to prevent from wear, to monitor the system state while reducing inspection costs.

Within the smart structures, piezoelectric actuators are one of the most widespread used in the industry. Piezoelectric materials are based on the electro-mechanical phenomenon which connects the mechanical properties of a material with its electrical ones. Piezoelectric materials produce a voltage when they are subjected to a mechanical stress, which is normally used by smart structures in order to act as a sensor. Piezoelectric materials also works the other way round, converting voltage difference into mechanical strain, which is typically used to act as an actuator.[3].

The appearance of the smart structures is the consequence of the constant work on improving structures by increasing its relevant characteristics. A key factor in this structure improvement was the introduction of composite materials. They are formed by a combination of two or more materials with the aim of improving the engineering properties that will exhibit separately any of the materials which forms it. Depending on its combination structure they are classified by: fiber, particulate, laminar, flake and filled. Among these classification, the most commonly used are the laminated composites, since they are ideal for those applications in which both high strength-to-weight and stiffness-to-weight ratios are needed. The individual layers consist of high-modulus, fibers material. Typical laminated composites are made of continuous and high-strength fiber prepregs (graphite, glass, boron, silicon carbide...) in a polymeric, metallic or ceramic matrix (epoxies, polyimides, alumina...).

Composite materials have been recently introduced into many engineering fields such as construction, shipping, bioengineering or automotive industries due to their advantages with respect to the traditional structural materials like steel, titanium, aluminum and different alloys: they exhibit high stiffness, thermal properties, fatigue life and corrosion and wear resistance. However the industry in which they have been more developed due to their wide use is the aerospace field. The reason behind this extended use is the possibility of weight reduction added to the advantages in properties already commented. In this field any reduction in the structure's weight imply a direct impact in cost savings due to the reduction in the fuel needed.

Within these industries in which composite materials are used, there are many components that can be treated as beams and can incorporate intelligent materials to improve their performance by taking advantage of the benefits of this new generation of materials. Helicopter rotors, wings, turbine blades, drive shafts or robot arms are examples of possible smart beams structures.

1.2 Objectives

This Undergraduate Thesis Project assesses the response of smart structures modeled as sandwich-structured composite beams with the inclusion of piezoelectric materials within the stacking sequence, being these beams subjected to a temperature difference or an electric field.

In order to accomplish this analysis, several partial objectives have been established:

- Development of a simplified model with the equations needed to accurately predict the vertical displacements and rotations exhibited by the beams due to the static loads at which they are exposed. This model covers the cases of presence of a temperature difference and/or an electric field.

- Further study of the capabilities of smart structures, specifically those made of piezoelectric materials. This objective includes the relation of the piezoelectric characteristics into a valid model for the motion description of composite beams.

The developed model enables a study to analyze the beam deflections produced under certain loads when the piezoelectric material deforms due to the influence of the electric field so as to compare them with the case when there is no electric field. The final goal is to see the control capability over the beam deflections by the inclusion of certain electric field and how it could be affected by the presence of a temperature difference.

1.3 Project description

This Undergraduate Thesis Project has been divided into six chapters, being the first of them this introduction.

Subsequently, the second chapter collects a bibliographic revision of the most relevant studies of the problems to be analyzed by some researchers in smart materials and structures and its applications and more specifically on the piezoelectric materials.

Afterwards, third chapter covers the development of the analytic model used to describe displacements and rotations produced in plates through the Classical Laminated Plate Theory, accounting for the piezoelectric and the temperature difference effects. This theory is extended to beams in chapter four, where the sandwich beam and its context is also described. The static displacements and rotations for a given stacking sequence are obtained under the separate presence

of an electric field and a temperature difference.

Consequently, the fifth chapter covers different studies that arise from the results obtained in the previous chapter, such as analysis of the effect of the stacking sequence used, the sensitivity to the sandwich core and the piezoelectric materials thicknesses. In addition voltage and temperature difference are analyzed together to see the how their simultaneous presence affect the beam response.

The main conclusions and the possible future studies are summarized in the sixth chapter. Finally, the bibliographic references needed for the execution of this Undergraduate Thesis Project are included, together with an appendix which includes an estimation of the total cost of this dissertation.

CHAPTER 2

Background

2.1 Smart structures

The use of intelligent structures has been extended in the past three decades. They have moved from being restricted just for research applications towards a more and more spread industrialization. This evolution in the technology has implied a change in the definition of a smart material. Earlier, smart material was defined as the material which responds to its environments in a certain amount of time. However, its definition has been expanded to those materials that are able to receive, process and transmit a stimulation from the environment[4].

Smart structures integrates in one architecture the key elements which entail an active system, in addition to the processes that relates them. They possess an embedded mechanism which enables them to process and control the internal information received to either recognize the surrounding condition and act as sensors or an actuator which enables the system the capability to react against the environment stimuli. Some smart materials have both mechanisms and can act as sensors or as actuators depending on the working conditions. The typical scheme of the data flow within a smart system is detailed in Figure 2.1.1[5].

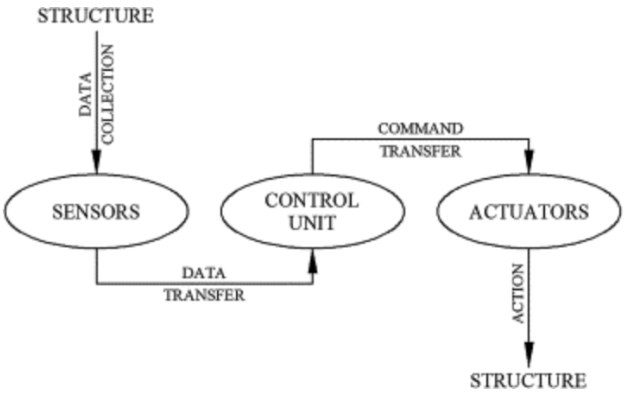

Figure 2.1.1: Smart system components

Several authors have developed different classifications of smart structures

depending on the criteria used.

Rogers[6] defined a classification based on the functionality: sensory, adaptive, controlled, active and smart structures. Sensory structures posses materials which act as sensors to monitor the state of the system. On the other hand, adaptive structures posses actuators in order to modify the system status. Controlled structures have both sensors and actuators integrated in a feedback loop system with the aim of monitoring the system characteristics, so that they are the resultant combination of the sensory and the adaptive structures. Moreover, active structures are controlled structures with sensors and actuators highly integrated into the system, offering structural functionality besides the control function. Finally, the smart structures are those active structures with either a highly integrated architecture or hierarchic control framework. The relationship established among this classification is clearly defined with Figure 2.1.2, taken from Rogers[6].

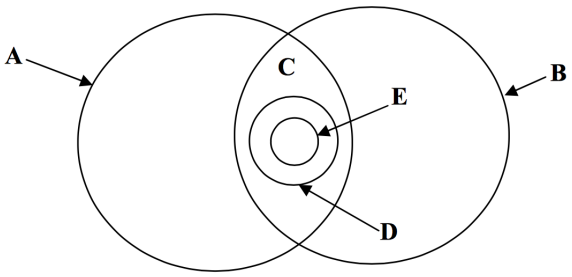

A: Sensory structures; **B:** Adaptive structures; **C:** Controlled structures;
D: Active structures; **E:** Intelligent structures.

Figure 2.1.2: Rogers' classification of smart structures

Similar to the Rogers' classification, there is another wider classification regarding the structure function: active and passive smart structures. On one hand, according to Fairweather[7] active smart structures are those made of materials with the ability to modify their physical characteristics under the application of electric, thermal or magnetic fields, so that they possess the inherent capacity to convert energy. On the other hand, passive smart structures are based on materials which can act as sensors but not as actuators or transducers.

Furthermore, there is an additional classification based on the physical domains involved in the energy conversion accomplished by the intelligent structure. An example of the relationship among three of the main physical domains involved in smart structures (mechanical, electrical and thermal) with their state variables and the physical property produced by their coupling is shown in Figure 2.1.3, which is extracted from Donald[8]. There are other couplings produced by another physical domains such as magnetic or optical. These physical phenomenons are the basis behind the most commonly used intelligent materials, which are shown in the rectangles of Figure 2.1.4, which is extracted from Kamila[4].

Among the most common intelligent materials detailed in Figure 2.1.4, the most versatile are the piezoelectrics and the magneto-strictives, which can act as

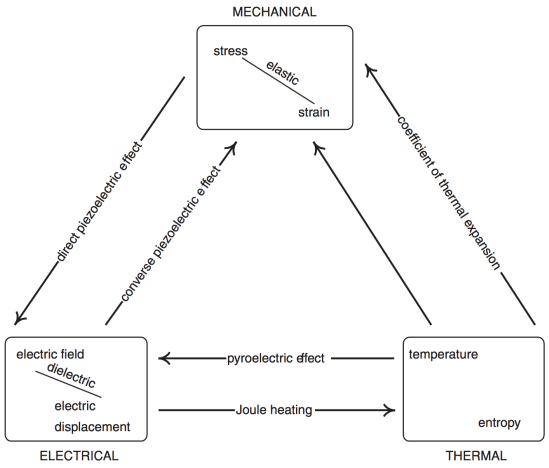

Figure 2.1.3: Coupling between physical domains

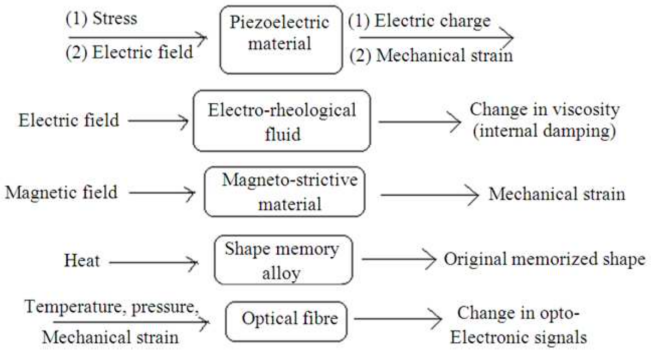

Figure 2.1.4: Most common smart materials with their associated stimuli

sensors and actuators. Shape memory alloys can only work as actuators, as electro-rheological and magneto-rheological fluids, which are mainly used for the active vibration. Optical fibers are used predominately as sensors, being the most popular one the fiber Bragg Grating sensors. A brief background of their applications and the physics behind them are explained hereunder, being the piezoelectric materials deeply detailed in next section.

The electrorheological fluids are the ones which exhibit a change in viscosity in the presence of a electric field. The electrorheological effect is produced due to the difference in the dielectric constant between the solid particles and the liquid in a colloid. Electric polarization resulted in the fluid molecules can arise in two different ways from an applied electric field[9].

The first electric polarization process is the dielectric electrorheological (DER) effect, which is produced due to the mechanism established when the colloid is subjected to an electric field, in which the solid particles and the liquid will have different dipole moments, whose interaction tends to form columns along the applied field direction, increasing the fluid viscosity. The second polarization procedure is called the giant electrorheological (GER) effect, which was recently discovered by Wen et al. in 2003[10]. It is created by the alignment of the molecular

dipoles, which initially are randomly oriented, in a silicone oil with urea coated nanoparticles of Barium Titanium Oxalate suspended on it. GER fluids are able to sustain higher yield strengths than other ER fluids [11] [12].

The actuator capability of electrorheological fluids has been applied to active automotive devices such as engine dampers, shock absorbers, clutches or hydraulic valves, which are controlled by regulating the electric field applied. The sensor capacity is also used to monitor the mechanical vibration signals[13].

Similar to electrorheological fluids, magnetorheological fluids can also change their viscosity in several orders of magnitude within a short period of time due to the presence of a magnetic field. Magnetorheological fluids contain ferromagnetic or paramagnetic particles, which are aligned when the fluid is exposed to a magnetic field[9].

Magnetorheological fluids are under an intensive study, being used in industries such as the aerospace or the automotive due to their good performance as dampers, in which the dissipation factor can be adjusted by adapting the magnetic field intensity crossing the fluid[14]. Besides, magnetorheological fluids are involved in a technique for improving surface finish of optical materials, magnetorheological finishing (MRF). In this technology, the magnetorheological fluid generates the energy needed for the surface polishing, achieving a reduction of the surface roughness up to less than 10 Å[15].

Moreover, magneto-strictives materials are based on a phenomenon called magnetostriction, discovered in 1842 by James Joule[16]. It is caused by the rotation of small magnetic field domains leading to internal strains which generates contraction or stretching in the structure. So as to keep the material volume, the cross-section is either increased or reduced, depending whether the material is contracting or stretching respectively, which is determined by the direction of magnetic field[17].

Terfenol-D is one of the magnetostrictive material with largest strain and force output, so that its applications have been under study. It has been found to work well as an actuator in those applications requiring large displacements. Due to the reciprocal nature of magnetostriction, they are also used as sensors. Their applications as actuators include motors, broadband shakers, surgical instruments or sonar transducers and as sensors hearing aids, load cells, accelerometers, magnetometers or torque sensors[18].

Besides, shape memory alloys (SMA) are also one of the most common smart materials, whose active capacity is provided thanks to the mechanical-thermal fields coupling. It is based on the reversed transformation process between the two different phases of these alloys, which if ordered from lower to higher temperature are martensite and austenite phases. An alloy subjected to an stress under low temperature (i.e. in martensitic phase) will exhibit deformation, which will be kept when load is released. If a heat process above the austenite finish

temperature is applied consequently, austenite will be generated with a recovery of the initial shape, which will be kept when cooling down below the martensitic finish temperature, resulting in martensite with the original shape[19] [20].

Shape memory effect was discovered in 1932 by Arne Olander in a gold-cadmium alloy[21]. This effect was afterwards demonstrated in a nickel-titanimum alloy with the development of NiTiNOL (*Nickel Titanium-Naval Ordnance Laboratory*) by Buehler et al. in 1963[22]. The good behavior observed in Nitinol, led to an intensive study of shape memory alloys properties and applications due to the possibilities it could offer. Among them, several important achievements were the detection that Cu and Fe as a good addition to the NiTi alloy in order to decrease the phase transition temperatures, the studies regarding High Temperature SMAs as the ones of Otsukaa[23] or the improving in the fatigue properties of NiTiCu[24].

Applications of shape memory alloys within the industry have been developed since 1960s with the discovery of Nitinol, although their use has been intensified since 1990s. SMAs have been applied to systems in the mechanical, the medical and the aerospace fields, such as in air conditioning vents, valves, medical wires, pipe couplings, appliance controllers or electronic connectors. The requirements for the application in some fields like the aerospace industry, in which the actuation is affected by a high temperature working conditions, have produced an attraction for the application of High Temperature SMA. While "classical" SMAs posses low frequency actuation, Magnetic SMA have been found to enable a high frequency actuation, so that they are under study for those application in which the actuation requires high frequency[20][25].

Finally, the last group within the most common smart materials indicated in Figure 2.1.4 are the fiber Bragg Grating (*FBG*). The currently used FBGs are the consequence of the evolution in the knowledge of photosensitivity, firstly discovered by Ken Hill in 1978[26]. The photosensitivity consists of the induced permanent change in the refractive index of a material, which is generated when it is subjected to light. In this process certain wavelengths are reflected while others are transmitted[27].

The FBGs are massively used in the telecommunication industry, specially in notch filters, multiplexings and demultiplexings. Nevertheless they are also used as sensors in other industries due to their multiplexing nature, which allow the simultaneous measure of different parameters within the same fiber[28].

Furthermore, there is a complete set of potential benefits that can be achieved with the introduction within the industry of the previously mentioned smart materials. One of the most promising advantages which can imply more impact on the industry is the capability of monitoring the status of the structure. It might entail a huge reduction in maintenance cost thanks to the control of cracks. There are different alternatives to control the damage of a structure with smart materials, which can be divided into two main groups[29].

The most traditional technique to monitor the structure status consists of a diagnosis with passive sensors, which measure different responses of the structure depending on whether it is damaged or not. It is difficult to estimate the severity of the damage, which can only be done by comparing the response with the simulations.

The second diagnosis technique is based on the use of embedded active sensors rather than passive, which are activated in order to take measurements. With this procedure it is possible to locate and analyze the damage severity. The materials with the two-directional nature with the possibility to act as sensors and actuators, such as magneto-strictive or piezoelectric materials, are normally used for this purposes.

The researches carried out to explore the capability of monitoring the material status has been also directed towards composite materials, which can be attractive for those industries with high concentration of composite components, such as the aerospace industry. Even though composite materials posses advantages in performance and weight compared to traditional metals, its reaction to loads and vibrations is different, generating crack growths which are not gradual anymore and are not as easily predictable as it occurs with the metallic materials. Therefore composite materials suffer from random and unpredictable damage, so that its monitoring process should be different than the one used for metallic components.

The method of monitoring a composite structure consists of embedding sensors and actuators within the composite layered architecture. Actuators excite the composite by generating waves which are received by the sensors. Any new crack apparition or crack growth will change the propagation pattern of the waves[30]. Several studies of this control application have been carried out with success, as the one made by Leng and Asundia to monitor the cure process of CFRP composite laminae with and without damage in real-time by using embedded fiber optic sensors such as extrinsic Fabry-Perot interferometer ($EFPI$) and fiber Bragg grating (FBG) sensors[31].

In addition to the monitor capacity of smart materials there are other smart materials capabilities, based on their sensing effectiveness, which can imply a great advance to the industry. Focusing on their acting capacity, which enables them to react against environment stimuli, there are three main applications with huge potential implication: shape morphing and noise and vibration suppression.

The noise or vibration suppression are achieved thanks to the emission of signals produced by the smart material reaction to a stimulus. The development of these applications and its employment can imply an important step in some industries. For instance in the civil engineering, it can be used to reduce the vibrations caused by an earthquake or in the aerospace industry where the control of the position, the control over frequency coalescence or the decrease in the noise emissions are of capital importance.

Regarding the vibration reduction, there are two main mechanisms. On one hand the passive technique is based on the use of a mechanism which can vary its properties, adding typically low energy to the system so that it cannot destabilize it. On the other hand, the active technique uses a set of actuators and sensors which interact between them controlling vibrations[29].

For noise mitigation, the smart materials with the dual capacity of actuating and sensing such as piezoelectric materials are the most commonly used. When they are used as sensors, they are able to detect any change in the air pressure produced by the sound waves. These pressure changes are converted into electric energy, which is supplied to other piezoelectric devices used as actuators with the purpose of emitting sound waves with opposite phase, so that sound can be dumped[32].

For the shape morphing, the aerospace industry is leading the researches in the implementation into aircraft and spacecraft structures of the deformation capacity of smart materials. The reason behind this interest is the susceptibility of the performance to the environment in these structures. Morphing technologies can increase the performance with significant weight savings by an automatic and real time manipulation of the aircraft and spacecraft characteristics to achieve an optimum configuration in each operating mission and at any environmental conditions.

The current morphing technology available has some disadvantages. Heavy motors and hydraulics are required to obtain the desired morphing movement and even with these devices significant structural changes are not easily achieved. With the introduction of smart materials, a fully integrated actuation can be obtained without the extra weight added with the installation of classical motors and actuators. Some examples of morphing applications with smart materials in the aerospace industry are now cited.

The developed technology based on shape memory alloys has enabled the construction of actuators that can imply a significant reduction in the weight. For instance, it has allowed to replace a 41 pound motor and gear box by a 1 pound of Nitinol actuator[33]. In short term, SMA are the most applicable smart material in the aerospace industry due to its efficiency and large energy storage capacity. Among the available SMA, Nitinol has been found to be the best candidate due to its availability and its superiority in performance compared to other SMA. Furthermore, acrylonitrile butadiene styrene plastic (ABS) provides a good solution for flexible skins as it is easily manipulated[34].

Another morphing program was a three-year project ended in 2005[35], which developed a reconfigurable engine nozzle fan chevron through a morphing technology based on shape memory alloy to enable efficient chevron with variable shape to optimize the engine performance and also to achieve a reduction of noise. Its validity has been checked through flight tests and static engine tests. Chevron

morphing idea is explained in Figure 2.1.5a. Its installation during a test in a Boeing 777 is shown in Figure 2.1.5b. These figures are extracted from Boeing and NASA reports[33] [36].

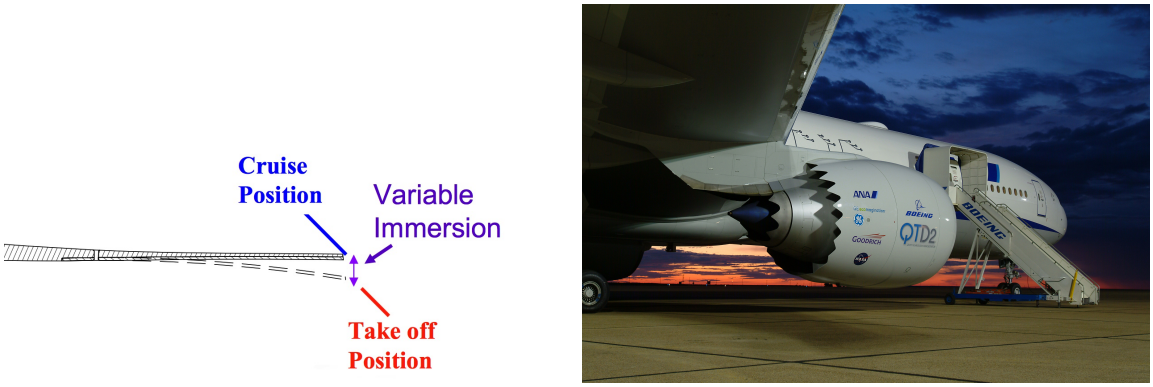

(a) (b)

Figure 2.1.5: Chevron SMA morphing technology, a) function scheme and b) installed in a Boeing's aircraft

However, in order to reduce the energy consumption required by the actuators, low stiffness of the morphing material during the deformation process is desired. Nevertheless, the morphing material should also possess enough out of plane bending stiffness to maintain the aerodynamic configuration suitable during the deformation process. Therefore engineering is focusing on creating materials with variable stiffness properties.

There are several technologies based on variable stiffness materials[37], such as the fish skin studied by Long et al.[38] or the skin with rubbery material, which presents high flexibility and elasticity[39]. However these new material technologies do not satisfy the all complete set of requirements needed for an aircraft wing: load bearing, accurate shape change and continuity and smoothness of the aerodynamic surface. Other variable stiffness material proposals are corrugated structures[40], with problems of limited deformability in one direction, or a styrene-based shape memory polymer composite (*SMPC*), studied by Lan et al.[41] in order to design a SMPC hinge actuation.

2.2 Piezoelectric structures

As seen in the previous section, piezoelectric materials are one of the smart materials most commonly used. The piezoelectric effect was discovered in 1880 by Pierre and Jacques Curie[42]. This phenomenon discovery was preceded by previous researches[43]. In 1815 Coulomb found that electricity might be produced with a pressure application. Years later, in 1820, Becquerel suggested that any charge produced by compression might have been caused by friction. He stated

that this production of charge could occur by stretching rubber or crystalline minerals.

The Curie's piezoelectric discovery was produced by the combination of Coulomb and Becquerel's researches and what Curie brothers knew about pyroelectricity. They found out that hemihedral crystals with oblique faces not only produce electrical poles when they are subjected to a variations in temperature along the hemihedral axes (pyroelectricity) but also when they are subjected to changes in pressure along these axes.

Upon the piezoelectric disclosure in 1880, efforts were made on understanding this effect[43]. In 1881, Gabriel Lippmann stated that the reversed phenomenon also exists (conversed piezoelectric phenomenon), i.e. when electricity is applied, a mechanical stress proportional to the existing voltage appears. One year later, the Curie brothers demonstrated experimentally the Lippmann's suggestion by obtaining that the coefficient for the conversed effect was identical to the direct one. In 1893, Kelvin developed theoretical models explaining the piezoelectric effect and Voigt[44] in 1910 published a definition of the piezoelectric governing equations as tensors. Afterwards, it was Mason in 1940 who extended the Kelvin's model applying it to crystal deformation.

The first applications of piezoelectric materials were made in 1917 during World War I with Langevin's development of a piezoelectric transducer to detect submarines through ultrasonic signals. In 1920 Joseph Valasek[45] discovered the ferroelectricity in the so-called Rochelle salt. Afterwards during World War II, research groups of both war parties separately worked on improving capacitor materials, discovering synthetic ceramic materials whose piezoelectric and dielectric properties are two order of magnitudes higher than the ones of the natural piezoelectric. It supposed a technological boom in the research of piezoelectric devices.

In 1945, the commercialization of piezoelectricity started when it was realized that barium titanate ($BaTiO_3$) was a ferroelectric material, easily manufactured and shaped with high piezoelectric constants achieved by the poling process. In this process, the material needs to be exposed to an initial voltage and heated above its Curie temperature, resulting in an alignment of the material dipoles so that then when it is subjected to a lower electric field, the dipoles react producing an expansion in the poling axis and a contraction in the perpendicular direction or the other way round, depending on the electric field sign[46].

Regarding the nature of piezoelectric materials, they can be divided into natural and man-made. The natural ones are crystal materials with piezoelectric properties such as quartz, Rochelle salt or the topaz. The man-made ceramics which exhibits piezoelectricity are the ones with the same crystal structure as perovskite ($CaTiO_3$). The most common man-made ceramics are barium titanate ($BaTiO_3$), lead titanate ($PbTiO_3$), lead zirconate titanate or PZT ($Pb[Zr_xTi_{1-x}]O_3$), being $0 < x < 1$, and potassium niobate ($KNbO_3$). There

are a more recently discovered family, which are the lead-free piezoceramics such as sodium potassium niobate ($(K, Na)NbO_3$) or bismuth ferrite ($BiFeO_3$)[47].

Despite the significant progress made with piezoelectric ceramics in the electromechanical coupling properties, several limitations in their performance have been found, such as lack of flexibility, brittleness or difficult attachment to curved structures. These flaws have been solved with the introduction of piezocomposites, where the piezoelectric material is the composite's fiber, which is embedded within the polymer matrix. Among them, the most commonly used are 1–3 piezocomposites, active-fiber composites (AFC) and macro-fiber composites (MFC)[48]. Piezoelectric composites have been classified depending on the connectivity pattern they present. There are ten different types, ranging from an unconnected pattern (0-0) to a pattern connected in the three dimensions in both phases (3-3)[49].

As commented before, the two-directional energy transformation capability of piezoelectric materials allow to use them as sensors, actuators or transducers. When they are used as sensors, strains are converted into electrical energy. The reversed conversion is used when they are applied as actuators, mechanical energy is generated from a given voltage. Finally, when they are used as transducers, the high frequency electrical energy is transformed into mechanical wave.

This versatile character of the piezoelectric materials enables to use them in many of the applications of smart structures mentioned in the previous section. Some of the applications of piezoelectric materials with the most implications to the industry are described hereunder.

Several studies have confirmed the piezoelectric's capacity of vibration damping. As it is the case of the experiment carried out over the spacecraft simulation of the Naval Postgraduate School, in which a positive position feedback controller made of piezoceramic actuators and sensors was designed to actively mitigate vibrations emitted in the pitch movement. For a single-mode excitation, damping could be enhanced significantly while for multiple-mode excitation only a limited damping increase was achieved [50]. Vibration reduction has also been achieved in a turbomachinery bladed disks with changing dynamics, in which the structural stiffness has been altered in vacuum in order to avoid resonance[51].

However it has been confirmed that noise reduction is not directly related with vibration reduction. It has been concluded in these studies that noise is barely affected by the vibration reduction produced by a piezoelectric material meanwhile if the goal is to achieve noise reduction, vibrations are greatly amplified[32]
.

In the automotive industry, piezoelectric materials have been applied for the active control of suspension. For instance, Toyota has developed the TEMS (Toyota Electronic Modulated Suspension) system, which seeks for an improvement in the handling and stability characteristics of the car. Five layers of piezoelectric materials are added to the piston rod of a shock absorber to detect

the stress caused by a bump, sending the produced voltage an actuator made of 88 layers of piezoelectric material[52].

Piezoelectric materials are also used for the control of the structure status. Studies as the one made by Alaimoa et al.[53], have demonstrated the applicability of piezoelectricity in the health monitoring of structures. In this study, the ability to sense the strain produced during the delamination process has been analyzed through the analysis of the piezoelectric electrical response. The impact location and strength of an impact in the composite material has been successfully identified.

All these industrial application examples can be used to summarize the recent interest on studies regarding the properties and capabilities of the piezoelectric materials and their implications within different industries. They reflect the current importance of the development of this new type of material together with other smart materials in order to achieve structures with better performance, which will enable the evolution of the industry.

CHAPTER 3

Model description

3.1 Displacements, strains and stress

Since composite laminae are characterized by having two dimensions with higher order of magnitude than their thickness, they can be treated as plates. Therefore, the Classical Laminated Plate Theory (CLPT) is a 2D theory that can be applied to the study of composite laminae, which is an extension based on the Classical Plate Theory. There is a more refined 2D theory, *first-order shear deformation theory (FSDT)*, which assumes a variable transverse shear strain along the thickness direction. However, it requires a shear correction factor, which is not easily determined since it depends on load, boundary conditions and the geometric characterization.

CLPT holds the Kirchhoff hypothesis[54], which is the extension of the Euler-Bernoulli beam theory by which any straight line perpendicular to the middle surface remains straight after deformation with no elongation exhibited, resulting in no transverse normal strain, $\epsilon_{zz}=0$. Additionally, these straight lines rotate in a way that they remain perpendicular to the middle thickness plane upon deformation, which implies no transverse shear strains is considered: $\epsilon_{xz}=0$ and $\epsilon_{yz}=0$. Besides the Kircchhoff hypothesis, the laminate layers are assumed to be perfectly bonded.

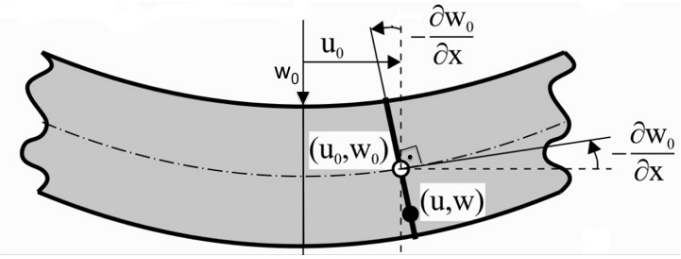

Figure 3.1.1: Deformed beam with Kirchhoff hypothesis

The general formulae needed to described the Classical Laminated Plate Theory is going to be detailed, following the development carried out by Reddy[55].

Based on Kirchhoff assumptions, the displacement field is

$$\begin{aligned} u(x,y,z,t) &= u_0(x,y,t) - z\frac{\partial w_0}{\partial x} \\ v(x,y,z,t) &= v_0(x,y,t) - z\frac{\partial w_0}{\partial y} \\ w(x,y,z,t) &= w_0(x,y,t) \end{aligned} \tag{3.1}$$

being u_0, v_0 and w_0 the displacements of the middle plane. So that the strains produced by these displacements are given by

$$\begin{aligned} \epsilon_{xx} &= \frac{\partial u}{\partial x} + \frac{1}{2}[\frac{\partial u}{\partial x}^2 + \frac{\partial v}{\partial x}^2 + \frac{\partial w}{\partial x}^2] \\ \epsilon_{yy} &= \frac{\partial v}{\partial y} + \frac{1}{2}[\frac{\partial u}{\partial y}^2 + \frac{\partial v}{\partial y}^2 + \frac{\partial w}{\partial y}^2] \\ \gamma_{xy} &= \frac{1}{2}[\frac{\partial u}{\partial y} + \frac{\partial v}{\partial x} + \frac{\partial u}{\partial x}\frac{\partial u}{\partial y} + \frac{\partial v}{\partial x}\frac{\partial v}{\partial y} + \frac{\partial w}{\partial x}\frac{\partial w}{\partial y}] \end{aligned} \tag{3.2}$$

Since strains and displacements are considered to be small, all products of two displacement gradients are zero except for $(\frac{\partial w}{\partial x})^2, (\frac{\partial w}{\partial y})^2$ and $\frac{\partial w}{\partial x}\frac{\partial w}{\partial y}$. As a consequence, the strain associated with the displacement field is

$$\begin{aligned} \epsilon_{xx} &= \frac{\partial u_0}{\partial x} + \frac{1}{2}(\frac{\partial w_0}{\partial x})^2 - z\frac{\partial^2 w_0}{\partial x^2} \\ \epsilon_{yy} &= \frac{\partial v_0}{\partial y} + \frac{1}{2}(\frac{\partial w_0}{\partial y})^2 - z\frac{\partial^2 w_0}{\partial y^2} \\ \gamma_{xy} &= \frac{1}{2}(\frac{\partial u_0}{\partial y} + \frac{\partial v_0}{\partial x} + \frac{\partial w_0}{\partial x}\frac{\partial w_0}{\partial y}) - z\frac{\partial^2 w_0}{\partial x \partial y} \end{aligned} \tag{3.3}$$

where the terms multiplied by z constitute the flexural strains $(\epsilon^1_{xx}, \epsilon^1_{yy}, \gamma^1_{xy})$ and the remaining ones are the membrane strains $(\epsilon^0_{xx}, \epsilon^0_{yy}, \gamma^0_{xy})$.

As stated before, no transverse normal and shear strains *(ϵ_{xz}=0, ϵ_{yz}=0 and ϵ_{zz}=0)* are considered due to the Kirchhoff assumptions made in the CLPT definition. Consequently for orthotropic layers, there are no associated transverse shear stresses (σ_{xz}=0, σ_{yz}=0). Additionally, even if the transverse normal stress σ_{zz} is not zero because of the Poisson effect, it can be neglected due to the fact that it does not appear on the equations of motion.

The rest of the stress field in the global system of coordinates are obtained by introducing the constitutive relations for the layer k with the strain produced by the thermal expansion and adding, in the case of the piezoelectric material, the stress experimented by the presence of the electric field E^P.

$$\begin{aligned} \begin{Bmatrix} \sigma_{xx} \\ \sigma_{yy} \\ \sigma_{xy} \end{Bmatrix}^{(k)} &= \begin{bmatrix} \bar{Q}_{11} & \bar{Q}_{12} & \bar{Q}_{16} \\ \bar{Q}_{12} & \bar{Q}_{22} & \bar{Q}_{26} \\ \bar{Q}_{16} & \bar{Q}_{26} & \bar{Q}_{66} \end{bmatrix}^{(k)} \left[\begin{Bmatrix} \epsilon_{xx} \\ \epsilon_{yy} \\ \gamma_{xy} \end{Bmatrix} - \begin{Bmatrix} \alpha_{xx} \\ \alpha_{yy} \\ 2\alpha_{xy} \end{Bmatrix} \Delta T \right] \\ &- \begin{bmatrix} 0 & 0 & \bar{e}_{31} \\ 0 & 0 & \bar{e}_{32} \\ 0 & 0 & \bar{e}_{33} \end{bmatrix}^{(k)} \begin{Bmatrix} E^P_x \\ E^P_y \\ E^P_z \end{Bmatrix}^{(k)} \end{aligned} \tag{3.4}$$

Being the plane-stress reduced stiffness for the orthotropic material, expressed in the local coordinates

$$Q_{11} = \frac{E_1}{1-\nu_{12}\nu_{21}}; \quad Q_{12} = \frac{\nu_{12}E_2}{1-\nu_{12}\nu_{21}} = \frac{\nu_{21}E_1}{1-\nu_{12}\nu_{21}};$$
$$Q_{22} = \frac{E_2}{1-\nu_{12}\nu_{21}}; \quad Q_{66} = G_{12} \tag{3.5}$$

and for the isotropic ones

$$Q_{11} = Q_{22} = \frac{E}{1-\nu^2}; \quad Q_{12} = Q_{21} = \frac{\nu E_1}{1-\nu^2}; \quad Q_{66} = \frac{E(1-\nu)}{2(1-\nu^2)} \tag{3.6}$$

Their transformations to the global coordinates are given by

$$\begin{aligned}
\bar{Q}_{11} &= Q_{11}cos^4\theta + 2(Q_{12}+2Q_{66})sin^2\theta cos^2\theta + Q_{22}sin^4\theta \\
\bar{Q}_{12} &= (Q_{11}+Q_{22}-4Q_{66})sin^2\theta cos^2\theta + Q_{12}(sin^4\theta + cos^4\theta) \\
\bar{Q}_{22} &= Q_{11}sin^4\theta + 2(Q_{12}+2Q_{66})sin^2\theta cos^2\theta + Q_{22}cos^4\theta \\
\bar{Q}_{16} &= (Q_{11}-Q12-2Q_{66})sin\theta cos^3\theta + (Q_{12}-Q_{22}+Q_{66})sin^3\theta cos\theta \\
\bar{Q}_{26} &= (Q_{11}-Q12-2Q_{66})sin^3\theta cos\theta + (Q_{12}-Q_{22}+Q_{66})sin\theta cos^3\theta \\
\bar{Q}_{66} &= (Q_{11}+Q_{22}-2Q_{12}-2Q_{66})sin^2\theta cos^2\theta + Q_{66}(sin^4\theta + cos^4\theta)
\end{aligned} \tag{3.7}$$

For the case of the thermal coefficients of expansion

$$\begin{aligned}
\alpha_{xx} &= \alpha_1 cos^2\theta + \alpha_2 sin^2\theta \\
\alpha_{yy} &= \alpha_1 sin^2\theta + \alpha_2 cos^2\theta \\
2\alpha_{xy} &= 2(\alpha_1-\alpha_2)sin\theta cos\theta
\end{aligned} \tag{3.8}$$

and for the piezoelectric modulus:

$$\begin{aligned}
\bar{e}_{31} &= e_{31}cos^2\theta + e_{32}sin^2\theta \\
\bar{e}_{32} &= e_{31}sin^2\theta + e_{32}cos^2\theta \\
\bar{e}_{36} &= 2(e_{31}-e_{32})sin\theta cos\theta
\end{aligned} \tag{3.9}$$

3.2 Virtual displacements

The governing equations are obtained through the virtual displacement principle (3.10) in order to derive the Euler-Lagrange equations

$$0 = \int_0^T (\delta U + \delta V - \delta K)dt \tag{3.10}$$

being δU the virtual strain energy, δV the virtual work generated by the applied forces and δK the virtual kinetic energy:

$$\delta U = \int_{\Omega_0} \int_{-\frac{h}{2}}^{\frac{h}{2}} [\sigma_{xx}(\delta\epsilon_{xx}^{(0)} + z\delta\epsilon_{xx}^{(1)}) + \sigma_{yy}(\delta\epsilon_{yy}^{(0)} + z\delta\epsilon_{yy}^{(1)}) + 2\sigma_{xy}(\delta\gamma_{xy}^{(0)} + z\delta\gamma_{xy}^{(1)})]dzdxdy \tag{3.11}$$

$$\begin{aligned}\delta V = &- \int_{\Omega_0} [q_b(x,y) + q_t(x,y)]\delta w_0(x,y)dxdy \\ &- \int_{\Gamma_\sigma} \int_{-\frac{h}{2}}^{\frac{h}{2}} [\hat{\sigma_{nn}}(\delta u_{0n} - z\frac{\partial \delta w_0}{\partial n}) + \hat{\sigma_{ns}}(\delta u_{0s} - z\frac{\partial \delta w_0}{\partial s}) + \hat{\sigma_{nz}}\delta w_0]dzds\end{aligned} \tag{3.12}$$

$$\delta K = \int_{\Omega_0} \int_{-\frac{h}{2}}^{\frac{h}{2}} \rho_0 \big[(\dot{u_0} - z\frac{\partial \delta \dot{w}_0}{\partial x})(\delta \dot{u_0} - z\frac{\partial \delta \dot{w}_0}{\partial x}) + (\dot{v_0} - z\frac{\partial \delta \dot{w}_0}{\partial y})(\delta \dot{v_0} - z\frac{\partial \delta \dot{w}_0}{\partial y}) + \dot{w}_0 \delta \dot{w}_0\big] dzdxdy \tag{3.13}$$

where q_b and q_t are the distributed forces at the bottom and the top respectively. ρ_0 is the lamina density, Ω_0 is the xy middle plane of the laminate, δu_{0n} and δu_{0s} are the normal and tangential virtual displacements and σ_{nn}, σ_{ns} and σ_{nz} are the stress components of a given laminate portion Γ_σ.

In order to integrate virtual work and energies along the thickness direction, some important elements are introduced: N_{xx},N_{yy},N_{xy} are the in-plane force resultants, M_{xx},M_{yy},M_{xy} are the moment resultants, Q_n is the transverse force resultant, I_0,I_1,I_2 are the mass moment of inertia and q is the total transverse load, $q = q_b + q_t$

$$\begin{Bmatrix} N_{xx} \\ N_{yy} \\ N_{xy} \end{Bmatrix} = \int_{-\frac{h}{2}}^{\frac{h}{2}} \begin{Bmatrix} \sigma_{xx} \\ \sigma_{yy} \\ \sigma_{xy} \end{Bmatrix} dz, \qquad \begin{Bmatrix} M_{xx} \\ M_{yy} \\ M_{xy} \end{Bmatrix} = \int_{-\frac{h}{2}}^{\frac{h}{2}} \begin{Bmatrix} \sigma_{xx} \\ \sigma_{yy} \\ \sigma_{xy} \end{Bmatrix} zdz \tag{3.14}$$

$$\begin{Bmatrix} \hat{N_{nn}} \\ \hat{N_{ns}} \end{Bmatrix} = \int_{-\frac{h}{2}}^{\frac{h}{2}} \begin{Bmatrix} \hat{\sigma_{nn}} \\ \hat{\sigma_{ns}} \end{Bmatrix} dz, \qquad \begin{Bmatrix} \hat{M_{nn}} \\ \hat{M_{ns}} \end{Bmatrix} = \int_{-\frac{h}{2}}^{\frac{h}{2}} \begin{Bmatrix} \hat{\sigma_{nn}} \\ \hat{\sigma_{ns}} \end{Bmatrix} zdz \tag{3.15}$$

$$\begin{Bmatrix} I_0 \\ I_1 \\ I_2 \end{Bmatrix} = \int_{-\frac{h}{2}}^{\frac{h}{2}} \begin{Bmatrix} 1 \\ z \\ z^2 \end{Bmatrix} \rho_0 dz, \qquad \hat{Q_n} = \int_{-\frac{h}{2}}^{\frac{h}{2}} \{\hat{\sigma_{nz}}\} dz \tag{3.16}$$

Taking into account these quantities, the principle of virtual work can be represented as

$$
\begin{aligned}
0 = \int_0^T \Bigg\{ \int_{\Omega_0} \Big[& N_{xx}\delta\epsilon_{xx}^{(0)} + M_{xx}\delta\epsilon_{xx}^{(1)} + N_{yy}\delta\epsilon_{yy}^{(0)} + M_{yy}\delta\epsilon_{yy}^{(1)} \\
& + N_{xy}\delta\gamma_{xy}^{(0)} + M_{xy}\delta\gamma_{xy}^{(1)} - q\delta w_0 - I_0(\dot{u}_0\delta\dot{u}_0 + \dot{v}_0\delta\dot{v}_0 + \dot{w}_0\delta\dot{w}_0) \\
& + I_1\Big(\frac{\partial\delta\dot{w}_0}{\partial x}\dot{u}_0 + \frac{\partial\dot{w}_0}{\partial x}\delta\dot{u}_0 + \frac{\partial\delta\dot{w}_0}{\partial x}\dot{v}_0 + \frac{\partial\dot{w}_0}{\partial x}\delta\dot{v}_0\Big) + I_2\Big(\frac{\partial\delta\dot{w}_0}{\partial x}\frac{\partial\dot{w}_0}{\partial y} + \frac{\partial\dot{w}_0}{\partial y}\frac{\partial\delta\dot{w}_0}{\partial y}\Big)\Big] dxdy \\
& - \int_{\Gamma_0} \Big(\hat{N_{nn}}\delta u_{0n} + \hat{N_{ns}}\delta u_{0s} - \hat{M_{nn}}\frac{\partial\delta w_0}{\partial n} - \hat{M_{ns}}\frac{\partial\delta w_0}{\partial s} + \hat{Q_n}\delta w_0 \Big) ds \Bigg\} dt
\end{aligned} \tag{3.17}
$$

Virtual strains can be expressed as a function of the displacements as it was done with true strains in (3.3)

$$
\begin{aligned}
\delta\epsilon_{xx}^{(0)} &= \frac{\partial\delta u_0}{\partial x} + \frac{\partial w_0}{\partial x}\frac{\partial\delta w_0}{\partial x}; \quad \delta\epsilon_{xx}^{(0)} = -\frac{\partial^2 w_0}{\partial\delta x^2} \\
\delta\epsilon_{yy}^{(0)} &= \frac{\partial\delta u_0}{\partial y} + \frac{\partial w_0}{\partial y}\frac{\partial\delta w_0}{\partial y}; \quad \delta\epsilon_{yy}^{(0)} = -\frac{\partial^2 w_0}{\partial\delta y^2} \\
\delta\gamma_{xy}^{(0)} &= \frac{\partial\delta u_0}{\partial y} + \frac{\partial\delta v_0}{\partial x} + \frac{\partial w_0}{\partial y}\frac{\partial\delta w_0}{\partial x} + \frac{\partial w_0}{\partial x}\frac{\partial\delta w_0}{\partial y}; \quad \delta\gamma_{xy}^{(1)} = -2\frac{\partial^2\delta w_0}{\partial x\partial y}
\end{aligned} \tag{3.18}
$$

Introducing the virtual strains as a function of the displacements on (3.17) and rearranging for each of the virtual displacement coefficients

$$
\begin{aligned}
0 = \int_0^T \Bigg\{ \int_{\Omega_0} \Big[& -\Big(\frac{\partial N_{xx}}{\partial x} + \frac{\partial N_{xy}}{\partial y} - I_0\ddot{u}_0 + I_1\frac{\partial\ddot{w}_0}{\partial x}\Big)\delta u_0 \\
& -\Big(\frac{\partial N_{xy}}{\partial x} + \frac{\partial N_{yy}}{\partial y} - I_0\ddot{v}_0 + I_1\frac{\partial\ddot{w}_0}{\partial y}\Big)\delta v_0 - \Big(\frac{\partial M_{xx}}{\partial xx} + 2\frac{\partial M_{xy}}{\partial xy} + \frac{\partial M_{yy}}{\partial yy} + \mathcal{N}(w_0) + q \\
& -I_0\ddot{w}_0 + I_1\frac{\partial\ddot{u}_0}{\partial x} - I_1\frac{\partial\ddot{v}_0}{\partial y} + I_2\frac{\partial^2\ddot{w}_0}{\partial x^2} + I_2\frac{\partial^2\ddot{w}_0}{\partial x^2}\Big)\delta w_0\Big] dxdy \\
& + \int_{\Gamma_0} \Big[(N_{xx}n_x + N_{xy}n_y)\delta u_0 + (N_{xy}n_x + N_{yy}n_y)\delta v_0 \\
& -\Big(\frac{\partial M_{xx}}{\partial x}n_x + \frac{\partial M_{xy}}{\partial y}n_x + \frac{\partial M_{yy}}{\partial y}n_y + \frac{\partial M_{xy}}{\partial x}n_y + \mathcal{P}(w_0) \\
& -I_1\ddot{u}_0 n_x - I_1\ddot{v}_0 n_y + I_2\frac{\partial\ddot{w}_0}{\partial x}n_x + I_2\frac{\partial\ddot{w}_0}{\partial y}n_y\Big)\delta w_0 \\
& -(M_{xx}n_x + M_{xy}n_y)\frac{\partial\delta w_0}{\partial x} - (M_{xy}n_x + M_{yy}n_y)\frac{\partial\delta w_0}{\partial y}\Big] ds \\
& - \int_{\Gamma_0} \Big(\hat{N_{nn}}\delta u_{0n} + \hat{N_{ns}}\delta u_{0s} - \hat{M_{nn}}\frac{\partial\delta w_0}{\partial n} - \hat{M_{ns}}\frac{\partial\delta w_0}{\partial s} + \hat{Q_n}\delta w_0 \Big) ds \Bigg\} dt
\end{aligned} \tag{3.19}
$$

where

$$
\mathcal{N}(w_0) = \frac{\partial}{\partial x}\left(N_{xx}\frac{\partial w_0}{\partial x} + N_{xy}\frac{\partial w_0}{\partial y} \right) + \frac{\partial}{\partial y}\left(N_{xy}\frac{\partial w_0}{\partial x} + N_{yy}\frac{\partial w_0}{\partial y} \right) \tag{3.20}
$$

$$\mathcal{P}(w_0) = \left(N_{xx}\frac{\partial w_0}{\partial x} + N_{xy}\frac{\partial w_0}{\partial y}\right)n_x + \left(N_{xy}\frac{\partial w_0}{\partial x} + N_{yy}\frac{\partial w_0}{\partial y}\right)n_y \tag{3.21}$$

When actual displacements are known, virtual displacements are zero. Equations of motion are obtained with Euler-Lagrange equations by setting virtual displacements to zero over the laminate middle plane Ω_0:

$$\begin{aligned}
\delta u_0 : \quad & \frac{\partial N_{xx}}{\partial x} + \frac{\partial N_{xy}}{\partial y} = I_0\frac{\partial^2 u_0}{\partial t^2} - I_1\frac{\partial^2}{\partial t^2}\left(\frac{\partial w_0}{\partial x}\right) \\
\delta v_0 : \quad & \frac{\partial N_{xy}}{\partial x} + \frac{\partial N_{yy}}{\partial y} = I_0\frac{\partial^2 v_0}{\partial t^2} - I_1\frac{\partial^2}{\partial t^2}\left(\frac{\partial w_0}{\partial y}\right) \\
\delta w_0 : \quad & \frac{\partial^2 M_{xx}}{\partial x^2} + 2\frac{\partial^2 M_{xy}}{\partial x \partial y} + \frac{\partial^2 M_{yy}}{\partial y^2} + \mathcal{N}(w_0) + q = I_0\frac{\partial^2 w_0}{\partial t^2} \\
& -I_2\frac{\partial^2}{\partial t^2}\left(\frac{\partial^2 w_0}{\partial x^2} + \frac{\partial^2 w_0}{\partial y^2}\right) + I_1\frac{\partial^2}{\partial t^2}\left(\frac{\partial u_0}{\partial x} + \frac{\partial v_0}{\partial y}\right)
\end{aligned} \tag{3.22}$$

3.3 Electric field and temperature variation

The temperature and electric field variations have to be modeled in such a way that they can be used by the theoretical model in order to account for the effects of the presence of any fluctuation in both parameters. They can be represented by the variation in temperature and electric field with respect to a reference value.

For the sake of simplicity in the calculations, the temperature variation has been assumed to depend only on the z-direction, which is the most relevant one for the bending problem. Additionally, this dependence on the z coordinate has been modeled to behave as a linear variation.

$$\Delta T = T_0 + zT_1 \tag{3.23}$$

Similarly to the temperature variation, voltage has been also assumed to be dependent on z direction. Specifically, due to the relation of the electric field E^P and the voltage V, the electric field distribution is assumed to be created by a quadratic distribution of the voltage difference along the beam thickness coordinate in order to produce also a linear electric field variation in the z coordinate:

$$V(z) = az^2 + bz + c \tag{3.24}$$

$$E_x^P = \frac{\partial V}{\partial x}; \quad E_y^P = \frac{\partial V}{\partial y}; \quad E_z^P = \frac{\partial V}{\partial z} \tag{3.25}$$

$$E_z^P = E_z^P(0) + zE_z^P(1) \tag{3.26}$$

3.4 Constitutive equations

Constitutive equations are established in order to relate force and moments to the strains produced by the beam displacement through the stress-strain relation (3.4).

$$\begin{Bmatrix} N_{xx} \\ N_{yy} \\ N_{xy} \end{Bmatrix} = \sum_{k=1}^{N} \int_{z_k}^{z_{k+1}} \begin{Bmatrix} \sigma_{xx} \\ \sigma_{yy} \\ \sigma_{xy} \end{Bmatrix} dz =$$

$$\begin{bmatrix} A_{11} & A_{12} & A_{16} \\ A_{12} & A_{22} & A_{26} \\ A_{16} & A_{26} & A_{66} \end{bmatrix} \left(\begin{Bmatrix} \epsilon^0_{xx} \\ \epsilon^0_{yy} \\ \gamma^0_{xy} \end{Bmatrix} - \begin{Bmatrix} \alpha_{xx} \\ \alpha_{yy} \\ 2\alpha_{xy} \end{Bmatrix} T_0 \right) + \begin{bmatrix} B_{11} & B_{12} & B_{16} \\ B_{12} & B_{22} & B_{26} \\ B_{16} & B_{26} & B_{66} \end{bmatrix} \left(\begin{Bmatrix} \epsilon^1_{xx} \\ \epsilon^1_{yy} \\ \gamma^1_{xy} \end{Bmatrix} - \begin{Bmatrix} \alpha_{xx} \\ \alpha_{yy} \\ 2\alpha_{xy} \end{Bmatrix} T_1 \right)$$

$$- \begin{bmatrix} 0 & 0 & F_{16} \\ 0 & 0 & F_{26} \\ 0 & 0 & F_{66} \end{bmatrix} \begin{Bmatrix} E^P_{x(0)} \\ E^P_{y(0)} \\ E^P_{z(0)} \end{Bmatrix} - \begin{bmatrix} 0 & 0 & G_{16} \\ 0 & 0 & G_{26} \\ 0 & 0 & G_{66} \end{bmatrix} \begin{Bmatrix} E^P_{x(1)} \\ E^P_{y(1)} \\ E^P_{z(1)} \end{Bmatrix} \tag{3.27}$$

$$\begin{Bmatrix} M_{xx} \\ M_{yy} \\ M_{xy} \end{Bmatrix} = \sum_{k=1}^{N} \int_{z_k}^{z_{k+1}} \begin{Bmatrix} \sigma_{xx} \\ \sigma_{yy} \\ \sigma_{xy} \end{Bmatrix} z dz =$$

$$\begin{bmatrix} B_{11} & B_{12} & B_{16} \\ B_{12} & B_{22} & B_{26} \\ B_{16} & B_{26} & B_{66} \end{bmatrix} \left(\begin{Bmatrix} \epsilon^0_{xx} \\ \epsilon^0_{yy} \\ \gamma^0_{xy} \end{Bmatrix} - \begin{Bmatrix} \alpha_{xx} \\ \alpha_{yy} \\ 2\alpha_{xy} \end{Bmatrix} T_0 \right) + \begin{bmatrix} D_{11} & D_{12} & D_{16} \\ D_{12} & D_{22} & D_{26} \\ D_{16} & D_{26} & D_{66} \end{bmatrix} \left(\begin{Bmatrix} \epsilon^1_{xx} \\ \epsilon^1_{yy} \\ \gamma^1_{xy} \end{Bmatrix} - \begin{Bmatrix} \alpha_{xx} \\ \alpha_{yy} \\ 2\alpha_{xy} \end{Bmatrix} T_1 \right)$$

$$- \begin{bmatrix} 0 & 0 & G_{16} \\ 0 & 0 & G_{26} \\ 0 & 0 & G_{66} \end{bmatrix} \begin{Bmatrix} E^P_{x(0)} \\ E^P_{y(0)} \\ E^P_{z(0)} \end{Bmatrix} - \begin{bmatrix} 0 & 0 & H_{16} \\ 0 & 0 & H_{26} \\ 0 & 0 & H_{66} \end{bmatrix} \begin{Bmatrix} E^P_{x(1)} \\ E^P_{y(1)} \\ E^P_{z(1)} \end{Bmatrix} \tag{3.28}$$

being

$$\begin{Bmatrix} A_{ij} \\ B_{ij} \\ D_{ij} \end{Bmatrix} = \sum_{k=1}^{N} \bar{Q}^{(k)}_{ij} \begin{Bmatrix} (z_{k+1} - z_k) \\ \frac{1}{2}(z^2_{k+1} - z^2_k) \\ \frac{1}{3}(z^3_{k+1} - z^3_k) \end{Bmatrix} \tag{3.29}$$

$$\begin{Bmatrix} F_{ij} \\ G_{ij} \\ H_{ij} \end{Bmatrix} = \sum_{k=1}^{N} \bar{e}^{(k)}_{ij} \begin{Bmatrix} (z_{k+1} - z_k) \\ \frac{1}{2}(z^2_{k+1} - z^2_k) \\ \frac{1}{3}(z^3_{k+1} - z^3_k) \end{Bmatrix} \tag{3.30}$$

Strains in (3.27) and (3.28) can be replaced by its equivalent displacements (3.3) in order to be able to insert the resultant forces and moments into the equations of motion (3.22). The complete set of governing expressions for the equations of motion are obtained as a function of the displacement components, the resultant moment and forces and the plate properties.

$$A_{11}(\frac{\partial^2 u_0}{\partial x^2}+\frac{\partial w_0}{\partial x}\frac{\partial^2 w_0}{\partial x^2})+A_{12}(\frac{\partial^2 v_0}{\partial x\partial y}+\frac{\partial w_0}{\partial y}\frac{\partial^2 w_0}{\partial x\partial y})$$
$$+A_{16}(\frac{\partial^2 u_0}{\partial x\partial y}+\frac{\partial^2 v_0}{\partial x^2}+\frac{\partial^2 w_0}{\partial x^2}\frac{\partial w_0}{\partial y}+\frac{\partial w_0}{\partial x}\frac{\partial^2 w_0}{\partial x\partial y})-B_{11}\frac{\partial^3 w_0}{\partial x^3}$$
$$-B_{12}\frac{\partial^3 w_0}{\partial x\partial y^2}-2B_{16}\frac{\partial^3 w_0}{\partial x^2\partial y}+A_{16}(\frac{\partial^2 u_0}{\partial x\partial y}+\frac{\partial w_0}{\partial x}\frac{\partial^2 w_0}{\partial x\partial y})+A_{26}(\frac{\partial^2 v_0}{\partial y^2}+\frac{\partial w_0}{\partial y}\frac{\partial^2 w_0}{\partial y^2})$$
$$+A_{66}(\frac{\partial^2 u_0}{\partial y^2}+\frac{\partial^2 v_0}{\partial x\partial y}+\frac{\partial^2 w_0}{\partial x\partial y}\frac{\partial w_0}{\partial y}+\frac{\partial w_0}{\partial x}\frac{\partial^2 w_0}{\partial y^2})-B_{16}\frac{\partial^3 w_0}{\partial x^2\partial y}-B_{26}\frac{\partial^3 w_0}{\partial y^3}$$
$$-2B_{66}\frac{\partial^3 w_0}{\partial x\partial y^2}-(\frac{\partial N^T_{xx}}{\partial x}+\frac{\partial N^T_{xy}}{\partial y}+\frac{\partial N^P_{xx}}{\partial x}+\frac{\partial N^P_{xy}}{\partial y})=I_0\frac{\partial^2 u_0}{\partial t^2}-I_1\frac{\partial^3 w_0}{\partial x\partial t^2} \quad (3.31)$$

$$A_{16}(\frac{\partial^2 u_0}{\partial x^2}+\frac{\partial w_0}{\partial x}\frac{\partial^2 w_0}{\partial x^2})+A_{26}(\frac{\partial^2 v_0}{\partial x\partial y}+\frac{\partial w_0}{\partial y}\frac{\partial^2 w_0}{\partial x\partial y})$$
$$+A_{66}(\frac{\partial^2 u_0}{\partial x\partial y}+\frac{\partial^2 v_0}{\partial x^2}+\frac{\partial^2 w_0}{\partial x^2}\frac{\partial w_0}{\partial y}+\frac{\partial w_0}{\partial x}\frac{\partial^2 w_0}{\partial x\partial y})-B_{16}\frac{\partial^3 w_0}{\partial x^3}$$
$$-B_{26}\frac{\partial^3 w_0}{\partial x\partial y^2}-2B_{66}\frac{\partial^3 w_0}{\partial x^2\partial y}+A_{12}(\frac{\partial^2 u_0}{\partial x\partial y}+\frac{\partial w_0}{\partial x}\frac{\partial^2 w_0}{\partial x\partial y})+A_{22}(\frac{\partial^2 v_0}{\partial y^2}+\frac{\partial w_0}{\partial y}\frac{\partial^2 w_0}{\partial y^2})$$
$$+A_{26}(\frac{\partial^2 u_0}{\partial y^2}+\frac{\partial^2 v_0}{\partial x\partial y}+\frac{\partial^2 w_0}{\partial x\partial y}\frac{\partial w_0}{\partial y}+\frac{\partial w_0}{\partial x}\frac{\partial^2 w_0}{\partial y^2})-B_{12}\frac{\partial^3 w_0}{\partial x^2\partial y}$$
$$-B_{22}\frac{\partial^3 w_0}{\partial y^3}-2B_{26}\frac{\partial^3 w_0}{\partial x\partial y^2}-(\frac{\partial N^T_{xy}}{\partial x}+\frac{\partial N^T_{yy}}{\partial y}+\frac{\partial N^P_{xy}}{\partial x}+\frac{\partial N^P_{yy}}{\partial y})=I_0\frac{\partial^2 v_0}{\partial t^2}-I_1\frac{\partial^3 w_0}{\partial y\partial t^2} \quad (3.32)$$

$$B_{11}(\frac{\partial^3 u_0}{\partial x^3}+(\frac{\partial^2 w_0}{\partial x^2})^2+\frac{\partial w_0}{\partial x}\frac{\partial^3 w_0}{\partial x^3})+B_{12}(\frac{\partial^3 v_0}{\partial x^2\partial y}+(\frac{\partial^2 w_0}{\partial x\partial y})^2+\frac{\partial w_0}{\partial y}\frac{\partial^3 w_0}{\partial x^2\partial y})$$
$$+B_{16}(\frac{\partial^3 u_0}{\partial x^2\partial y}+\frac{\partial^3 v_0}{\partial x^3}+\frac{\partial^3 w_0}{\partial x^3}\frac{\partial w_0}{\partial y}+2\frac{\partial^2 w_0}{\partial x^2}\frac{\partial^2 w_0}{\partial x\partial y}+\frac{\partial w_0}{\partial x}\frac{\partial^3 w_0}{\partial x^2\partial y})-D_{11}\frac{\partial^4 w_0}{\partial x^4}$$
$$-D_{12}\frac{\partial^4 w_0}{\partial x^2\partial y^2}-2D_{16}\frac{\partial^4 w_0}{\partial x^3\partial y}+2B_{16}(\frac{\partial^3 u_0}{\partial x^2\partial y}+\frac{\partial^2 w_0}{\partial x^2}\frac{\partial^2 w_0}{\partial x\partial y}+\frac{\partial w_0}{\partial x}\frac{\partial^3 w_0}{\partial x^2\partial y})+$$
$$2B_{26}(\frac{\partial^3 v_0}{\partial x\partial y^2}+\frac{\partial^2 w_0}{\partial x\partial y}\frac{\partial^2 w_0}{\partial y^2}+\frac{\partial w_0}{\partial y}\frac{\partial^3 w_0}{\partial x\partial y^2})+2B_{66}(\frac{\partial^3 u_0}{\partial x\partial y^2}+\frac{\partial^3 v_0}{\partial x^2\partial y}+\frac{\partial^3 w_0}{\partial x^2\partial y}\frac{\partial w_0}{\partial y}+$$
$$(\frac{\partial^2 w_0}{\partial x\partial y})^2+\frac{\partial w_0}{\partial y}\frac{\partial^3 w_0}{\partial x\partial y^2})-2D_{16}\frac{\partial^4 w_0}{\partial x^3\partial y}-2D_{26}\frac{\partial^4 w_0}{\partial x\partial y^3}-4D_{66}\frac{\partial^4 w_0}{\partial x^2\partial y^2}$$
$$+B_{12}(\frac{\partial^3 u_0}{\partial x\partial y^2}+(\frac{\partial^2 w_0}{\partial x\partial y})^2+\frac{\partial w_0}{\partial x}\frac{\partial^3 w_0}{\partial x\partial y^2})+B_{22}(\frac{\partial^3 v_0}{\partial y^3}+(\frac{\partial^2 w_0}{\partial y^2})^2+\frac{\partial w_0}{\partial y}\frac{\partial^3 w_0}{\partial y^3})$$
$$+B_{26}(\frac{\partial^3 u_0}{\partial y^3}+\frac{\partial^3 v_0}{\partial x\partial y^2}+\frac{\partial^3 w_0}{\partial x\partial y^2}\frac{\partial w_0}{\partial y}+2\frac{\partial^2 w_0}{\partial x\partial y}\frac{\partial^2 w_0}{\partial y}+\frac{\partial w_0}{\partial x}\frac{\partial^3 w_0}{\partial y^3})-D_{12}\frac{\partial^4 w_0}{\partial x^2\partial y^2}$$
$$-D_{22}\frac{\partial^4 w_0}{\partial y^4}-2D_{26}\frac{\partial^4 w_0}{\partial x\partial y^3}+\mathcal{N}(w_0)+q-(\frac{\partial^2 M^T_{xx}}{\partial x^2}+2\frac{\partial^2 M^T_{xy}}{\partial y\partial x}+\frac{\partial^2 M^T_{yy}}{\partial y^2}+\frac{\partial^2 M^P_{xx}}{\partial x^2}$$
$$+2\frac{\partial^2 M^P_{xy}}{\partial y\partial x}+\frac{\partial^2 M^P_{yy}}{\partial y^2})=I_0\frac{\partial^2 w_0}{\partial t^2}-I_2\frac{\partial^2}{\partial t^2}(\frac{\partial^2 w_0}{\partial x^2}+\frac{\partial^2 w_0}{\partial y^2})+I_1\frac{\partial^2}{\partial t^2}(\frac{\partial u_0}{\partial x}+\frac{\partial v_0}{\partial y}) \quad (3.33)$$

Where N^T, M^T, N^P and M^P are the force and moment resultants from the temperature and electric field terms in the constitutive equations (3.27) and (3.28).

CHAPTER 4

Application of the model to beams

4.1 General equations

In this chapter the Classical Laminated Plate Theory, described in the previous chapter by the equations derived by Reddy[55], is going to be applied to beams. Some assumptions are introduced, which will simplify the algebra for the plate equations of motion.

In addition, a more specific study will be performed in order to apply the theoretical model over the beam bending problem. In order to make the reader see a practical and simplified approximation in the application of the theoretical model, two beam examples with different and basic boundary conditions are used: cantilever beam and simply supported beam.

The condition needed in order for a laminate to be treated as a beam is to have its length with higher in order of magnitude than its width. This laminate configuration implies that the displacements can be assumed to be only dependent on the coordinate in the direction of the beam length (x-coordinate) and time. The introduction of this assumption within the CLPT lead to a significant simplification and its application is valid since such a beam length implies the Poisson ratio and shear coupling on the deflection to be negligible.

Further simplifications can be achieved by using a symmetric stacking sequence. Notice in (3.29) and (3.30) that the contributions of B_{ij} and G_{ij} are null for a symmetric stacking sequence. Moreover, equations for bending are not coupled with torsion for these symmetric sequences, so that $M_{yy} = 0, M_{xy} = 0$.

Whenever a plate is loaded at its outer boundaries in the x and y directions, in-plane forces N_x, N_y and N_{xy} can be approximated to the values exhibited at the boundaries if the lateral displacements are small. Therefore, if there are no in-plane forces, the beam displacements in the xy plane, u_0 and v_0, are also zero so that the study can be reduced to the bending deflection problem.

With these assumptions, the Euler-Lagrange equation is reduced to

$$\frac{\partial^2 M_{xx}}{\partial^2 x} + q = I_0 \frac{\partial^2 w_0}{\partial^2 t} - I_2 \frac{\partial^4 w_0}{\partial^2 x \partial^2 t} \tag{4.1}$$

or

$$\frac{\partial^2 M}{\partial^2 x} + \tilde{q} = \tilde{I}_0 \frac{\partial^2 w_0}{\partial^2 t} - \tilde{I}_2 \frac{\partial^4 w_0}{\partial^2 x \partial^2 t} \tag{4.2}$$

being $M = bM_{xx}$; $\tilde{q} = bq$; $\tilde{I}_0 = bI_0$ and $\tilde{I}_2 = bI_2$.

Two different types of analyses are derived from the Euler-Lagrange equation, depending whether the displacements depend on time or not: static and dynamic analyses respectively.

Moreover, the complete set of equations of motion (3.31), (3.32) and (3.33) whose calculation was so involved, are significantly reduced to

$$M_{xx} = -D_{11} \frac{\partial^2 w_0}{\partial^2 x} - (D_{11}\alpha_{xx} + D_{12}\alpha_{yy} + 2D_{16}\alpha_{xy})T_1 - E^P_{z(1)} H_{16} \tag{4.3}$$

Notice that the intercept terms of the temperature and electric field effects are not reflected in the equations of motion for a symmetric beam due to the fact that study is reduced to the bending problem and additionally due to the cancellation of B and G matrices for this kind of beams.

Introducing $E_{xx} = \frac{b}{I_{yy} D^*_{11}}$, where $I_{yy} = \frac{1}{12} b h^3$
and $D^*_{11} = \frac{D_{22}D66 - D26^2}{D_{11}(D_{22}D_{66} - D^2_{26}) + D_{12}(D_{16}D_{26} - D_{12}D_{66}) + D_{16}(D_{12}D_{26} - D_{22}D_{16})}$

So that (4.3) turns into

$$M = -E_{xx} I_{yy} \left[\alpha_{xx} T_1 + \frac{\partial^2 w_0}{\partial^2 x} + D^*_{11} \left[D_{12}\alpha_{yy} T_1 + 2D_{16}\alpha_{xy} T_1 + E^P_{z(1)} H_{16} \right] \right] \tag{4.4}$$

Notice that the product $D^*_{11} D_{11}$ has been assumed to be equal to 1 due to the two different assumptions used: long beams and bending not coupled with torsion. This simplification introduces some minor error although it can be neglected.

Combining (4.4) with Euler-Lagrange (4.2)

$$-E_{xx} I_{yy} \frac{\partial^2}{\partial^2 x} \left[\alpha_{xx} T_1 + \frac{\partial^2 w_0}{\partial^2 x} + D^*_{11} \left[D_{12}\alpha_{yy} T_1 + 2D_{16}\alpha_{xy} T_1 + E^P_{z(1)} H_{16} \right] \right] + \tilde{q} = \tilde{I}_0 \frac{\partial^2 w_0}{\partial^2 t} - \tilde{I}_2 \frac{\partial^4 w_0}{\partial^2 x \partial^2 t} \tag{4.5}$$

If the static solution is analyzed

$$-E_{xx} I_{yy} \frac{\partial^2}{\partial^2 x} \left[\alpha_{xx} T_1 + \frac{\partial^2 w_0}{\partial^2 x} + D^*_{11} \left[D_{12}\alpha_{yy} T_1 + 2D_{16}\alpha_{xy} T_1 + E^P_{z(1)} H_{16} \right] \right] + \tilde{q} = 0 \tag{4.6}$$

By solving (4.6), the static vertical displacement is found at any point along the length direction

$$w_0(x) = \int_0^x \left(\int_0^\eta \left[\int_0^\epsilon \left(\int_0^\phi \frac{\tilde{q}(\mu)}{EI} d\mu \right) d\phi - \alpha_{xx} T_1 - D_{11}^* \big[D_{12}\alpha_{yy} T_1 + 2D_{16}\alpha_{xy} T_1 + E_{z(1)}^P H_{16} \big] \right] d\epsilon \right) d\eta + c_1 \frac{x^3}{3} + c_2 \frac{x^2}{2} + c_3 x + c_4 \tag{4.7}$$

and the rotation

$$\theta(x) = \frac{\partial w_0(x)}{\partial x} \tag{4.8}$$

Once vertical displacement and rotation at a given point are known, the vertical displacement at any other point is calculated by

$$w_B(x) = w_A(x) - \theta_A(x_B - x_a) - \int_A^B \frac{M_{xx}}{EI}(x_b - x) dx \tag{4.9}$$

When an uniform pressure q_0 is applied the vertical displacement, rotation, moment distribution and shear force result respectively in:

$$w_0(x) = \frac{q_0 b}{24EI} x^4 - \left[\alpha_{xx} T_1 + D_{11}^* \big(D_{12}\alpha_{yy} T_1 + 2D_{16}\alpha_{xy} T_1 + E_{z(1)}^P H_{16} \big) \right] \frac{x^2}{2} + c_1 \frac{x^3}{3} + c_2 \frac{x^2}{2} + c_3 x + c_4 \tag{4.10}$$

$$\theta(x) = \frac{q_0 b}{6EI} x^3 - \left[\alpha_{xx} T_1 + D_{11}^* \big(D_{12}\alpha_{yy} T_1 + 2D_{16}\alpha_{xy} T_1 + E_{z(1)}^P H_{16} \big) \right] x + c_1 x^2 + c_2 x + c_3 \tag{4.11}$$

$$M(x) = \frac{q_0 b}{EI} \frac{x^2}{2} + 2c_1 x + c_2 \tag{4.12}$$

$$Q(x) = \frac{\partial M(x)}{\partial x} = \frac{q_0 b}{EI} x + 2c_1 \tag{4.13}$$

The boundary conditions of the two simple cases which are going to be studied in this Undergraduate Thesis Project are introduced next.

4.1.1 Cantilever beam

The cantilever beam is characterized by being clamped at one of its edges and be free at the other one. The main implications over the beam status of this type of boundary conditions are:

- Clamped at x=0: $w_0(0) = 0$ and $\frac{\partial w_0(x)}{\partial x}(0) = 0$
- Free at x=L: $M(L) = 0$ and $Q(L) = 0$

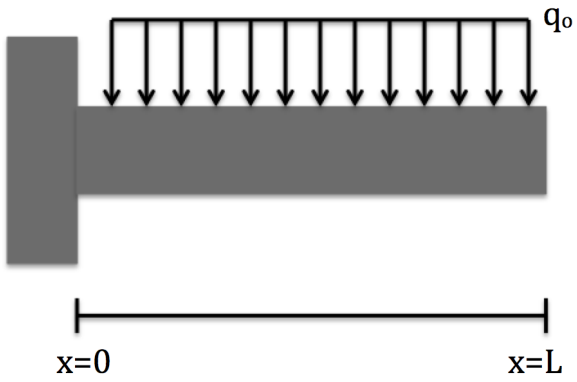

Figure 4.1.1: Cantilever beam subjected to uniform load

From $\frac{\partial w_0(x)}{\partial x}(0) = 0$, c_3 is known to be 0. The same occurs to c_4 with $w_0(0) = 0$. From the free end c_1 and c_2 are obtained: $c_1 = -\frac{q_0 bL}{2EI}$ and $c_2 = \frac{q_0 bL^2}{2EI}$

Therefore the vertical displacement and rotation at any of the x-direction location are:

$$w_0(x) = -\left[\alpha_{xx}T_1 + D_{11}^*\left(D_{12}\alpha_{yy}T_1 + 2D_{16}\alpha_{xy}T_1 + E_{z(1)}^P H_{16}\right)\right]\frac{x^2}{2} + \frac{q_0 b}{24EI}x^4 - \frac{q_0 bL}{6EI}x^3 + \frac{q_0 bL^2}{4EI}x^2 \tag{4.14}$$

$$\theta(x) = -\left[\alpha_{xx}T_1 + D_{11}^*\left(D_{12}\alpha_{yy}T_1 + 2D_{16}\alpha_{xy}T_1 + E_{z(1)}^P H_{16}\right)\right]x + \frac{q_0 b}{6EI}x^3 - \frac{q_0 bL}{2EI}x^2 + \frac{q_0 bL^2}{2EI}x \tag{4.15}$$

Consequently both the displacement and the rotation are maximum at x=L

$$w_{0_{max}} = -\left[\alpha_{xx}T_1 + D_{11}^*\left(D_{12}\alpha_{yy}T_1 + 2D_{16}\alpha_{xy}T_1 + E_{z(1)}^P H_{16}\right)\right]\frac{L^2}{2} + \frac{3q_0 bL^4}{24EI} \tag{4.16}$$

$$\theta_{max} = -\Big[\alpha_{xx}T_1 + D_{11}^*\big(D_{12}\alpha_{yy}T_1 + 2D_{16}\alpha_{xy}T_1 + E_{z(1)}^P H_{16}\big)\Big]L + \frac{q_0 b L^3}{6EI} \quad (4.17)$$

4.1.2 Simply supported beam

The simply supported boundary conditions exhibits no vertical displacement and moment at the support point, $w_0 = 0$ and $M = 0$. The null moment at the ends produces $c_2 = 0$ and $c_1 = -\frac{q_0 b L}{4EI}$. In addition from the restriction of the vertical displacement, the rest of the boundary condition constants are found out: $c_4 = 0$ and $c_3 = \big[\alpha_{xx}T_1 + D_{11}^*(D_{12}\alpha_{yy}T_1 + 2D_{16}\alpha_{xy}T_1 + E_{z(1)}^P H_{16})\big]\frac{L}{2} + \frac{q_0 b L^3}{24EI}$

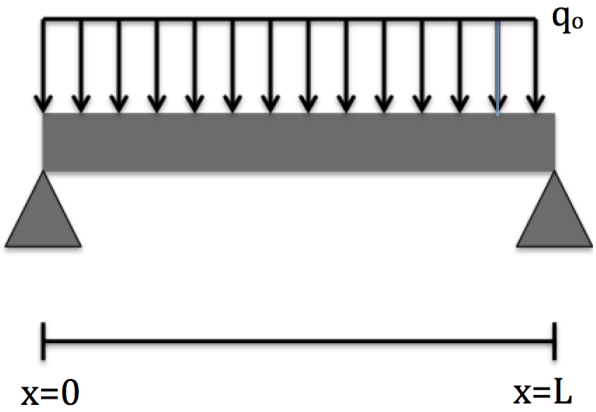

Figure 4.1.2: Simply supported beam subjected to uniform load

The vertical displacement and rotation are:

$$w_0(x) = -\Big[\alpha_{xx}T_1 + D_{11}^*\big(D_{12}\alpha_{yy}T_1 + 2D_{16}\alpha_{xy}T_1 + E_{z(1)}^P H_{16}\big)\Big]\left(\frac{x^2}{2} - \frac{Lx}{2}\right) + \frac{q_0 b}{24EI}x^4 - \frac{q_0 b L}{12EI}x^3 + \frac{q_0 b L^3}{24EI}x \quad (4.18)$$

$$\theta(x) = -\Big[\alpha_{xx}T_1 + D_{11}^*\big(D_{12}\alpha_{yy}T_1 + 2D_{16}\alpha_{xy}T_1 + E_{z(1)}^P H_{16}\big)\Big]\left(x - \frac{L}{2}\right) + \frac{q_0 b}{6EI}x^3 - \frac{q_0 b L}{4EI}x^2 + \frac{q_0 b L^3}{24EI} \quad (4.19)$$

being the maximum displacement located at $x = \frac{L}{2}$ and the maximum rotation at $x = 0$ and $x = L$:

$$w_{0max} = -\Big[\alpha_{xx}T_1 + D_{11}^*\big(D_{12}\alpha_{yy}T_1 + 2D_{16}\alpha_{xy}T_1 + E_{z(1)}^P H_{16}\big)\Big]\frac{L}{8} + \frac{5q_0 b L^4}{384EI}x \quad (4.20)$$

$$\theta_{max} = \alpha_{xx} T_1 \frac{L}{2} + D_{11}^* \frac{L}{2}\left(D_{12}\alpha_{yy}T_1 + 2D_{16}\alpha_{xy}T_1 + E_{z(1)}^P H_{16}\right) + \frac{q_0 b L^3}{24EI}$$
$$\theta_{max} = -\alpha_{xx} T_1 \frac{L}{2} - D_{11}^* \frac{L}{2}\left(D_{12}\alpha_{yy}T_1 + 2D_{16}\alpha_{xy}T_1 + E_{z(1)}^P H_{16}\right) - \frac{q_0 b L^3}{24EI} \quad (4.21)$$

4.2 Problem description

The problem to be studied is an Euler-Bernoulli sandwich beam of thickness h, length L and width w. It is made of an isotropic core plus N orthotropic laminae, each one oriented a given angle θ_k with a local coordinates (x_1^k,x_2^k,x_3^k) and assumed to be of uniform thickness. A piezoelectric ceramic material is added to the stacking sequence, which is set to be symmetric in order to be able to use the simplifications established in the previous chapter. The global axis is taken from the beam middle plane with z-axis being positive downwards.

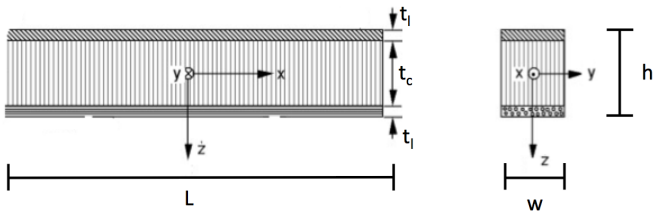

Figure 4.2.1: Sandwich beam

The beams to be studied are defined so that w=2h, being h and w the beam thickness and width respectively, so that both parameters will depend on the type of materials used. However the length is equal to 1.5 meters and kept constant for all the studies, regardless the laminate materials and stacking sequences used in order to compare deflections and rotations. Additionally the thickness of the core t_c is set to be four times the resulting thickness of the sum of the upper and lower stacking sequences produced by the superposition of the composite laminae together with the piezoelectric materials used, t_l.

Regardless of the case, it is important to ensure that the assumption of $L >> w$ is satisfied for any stacking sequence and material in order to guarantee the approximations made during the development of the application of the theoretical model to beams.

Two different types of fibers have been used in the study, both of them with epoxy resin. One laminate with pre-preg carbon fiber (AS4/epoxy fiber, 3501-6 epoxy matrix) and another with filament winding glass fiber (Silenka E-Glass 1200tex fiber, MY750/HY917/DY063 epoxy matrix). In addition, a variety of

lead zirconate titanate (*PZT-5H*) is inserted within the stacking sequence due to its piezoelectric behavior. Finally a PVC foam has been selected for the beam core. The most relevant properties of these different materials used are described in Table 4.2.1, whose values are taken from [56] and [58].

Properties	Fiber: AS4/epoxy Matrix: 3501-6 epoxy	Fiber: Silenka E-Glass 1200tex Matrix: MY750/ HY917/DY063 epoxy	DIAB Klegecell R 100 Rigid Closed Cell PVC Foam	PZT-5H 3195HD
$E_1(GPa)$	126	45.6	-	-
$E_2(GPa)$	11	16.2	-	-
$E(GPa)$	-	-	0.16	60
ν_{12}	0.28	0.278	-	-
ν	-	-	0.32	0.31
$G_{12}(GPa)$	6.6	5.85	-	-
$G(GPa)$	-	-	6.06 10^{-2}	22.9
$\alpha_1(10^{-6}/^oC)$	-1	8.6	-	-
$\alpha_2(10^{-6}/^oC)$	26	26.4	-	-
$\alpha(10^{-6}/^oC)$	-	-	35	3
$e_{31}(C/m^2)$	-	-	-	-10.4
$\rho(kg/m^3)$	1.58 10^3	-	100	7.8 10^3
Thickness (mm)	0.134	0.25	t_c	0.3175

Table 4.2.1: Properties of laminate, core and piezoelectric materials.

Among the different properties, one may notice that for the case of the piezoelectric material, only e_{31} is needed since the piezoelectric material is located at 0^o in (3.9). Additionally, the core thickness has not being defined since it depends on the thickness of the laminae used in each of the studies.

The different stacking sequences proposed are eight laminae with fibers aligned at 0^o, combined in different order with eight laminae with fibers at 90^o also and the same number of layers of piezoelectric materials. Both types of laminate materials selected will be analyzed separately and not mixed within the same stack. The geometry of each of the beams is detailed in Figure 4.2.2.

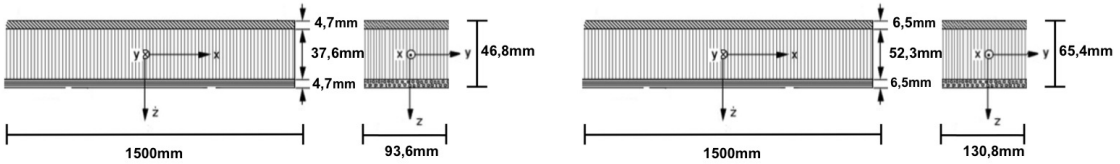

(a) (b)

Figure 4.2.2: Beam geometry definition for a) AS4/epoxy laminae and b) E-Glass/epoxy laminae.

The study is accomplished with the beam being subjected to a load uniformly distributed along the beam surface, q_0.

Furthermore, in order to asses the movement control, several temperature and electric field conditions are applied to different stacking sequences in order to see how the response is affected by them. The analysis is firstly done separately in order to assess properly the influence of each parameters for both laminae materials proposed.

The temperature study is performed by modeling the temperature difference between the upper and the bottom beam surfaces as a linear variation in the range of -20°C to 20°C.

The electric field at which the beam is subjected is modeled as a direct current (DC) voltage difference, evolving from null to certain value at which the PZT-5H can be exposed, as it is shown in Figure 4.2.3, which is extracted from Pacheco et al. [57]. This value has been decided to be 350 kV/m in order not to analyze the most extreme for the piezoelectric material, ensuring a margin of safety.

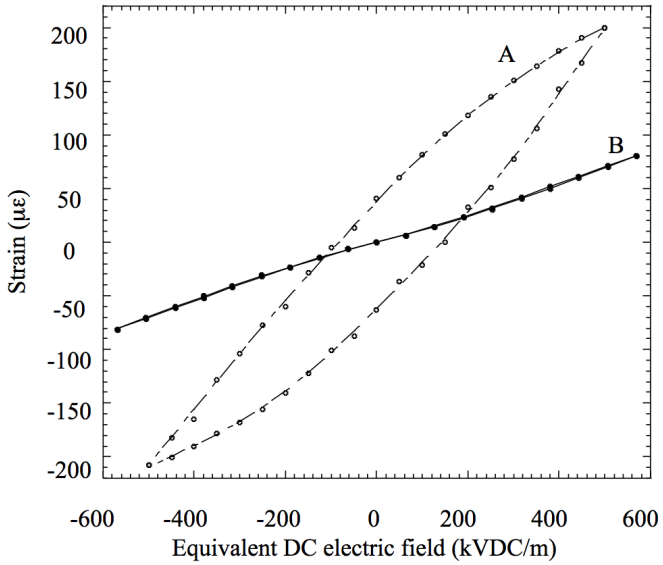

Figure 4.2.3: Comparison between the strain response of PZT-5H (curve A) and PZT-4 (curve B) piezoelectric ceramic types under an applied DC voltage.

4.3 Movement control

In this section the analysis of the temperature and electric field sensitivity is done separately for a $[0/90/p/0/90/p]_{4S}$ sequence in order to asses the dependence of the beam to these external factors and to study how one could take advantage of these dependence in order to be able to control the beam movement.

4.3.1 Voltage variation

The evolution of the maximum displacement and rotation as a function of the applied electric field for both laminae materials with $[90/0/p/90/0/p]_{4S}$ selected as the stacking sequence to be studied in this section are shown in following graphs.

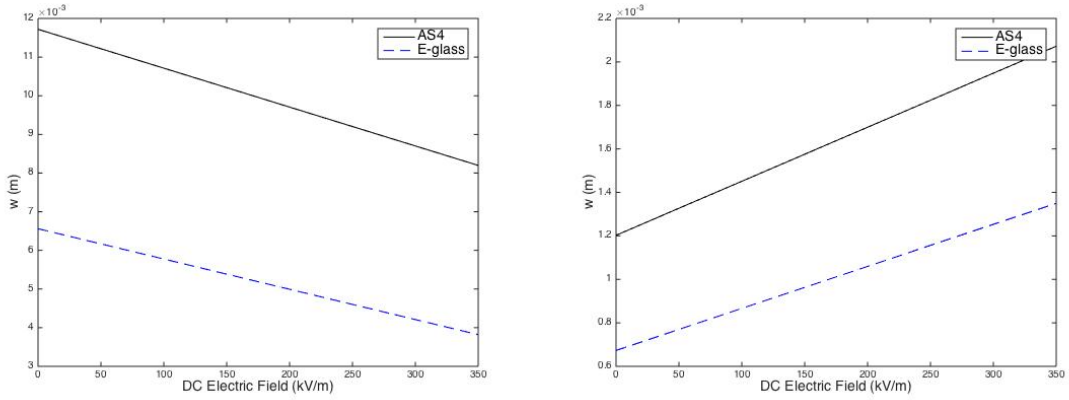

(a) (b)

Figure 4.3.1: Vertical displacement for $[90/0/p/90/0/p]_{4S}$ laminate in a) cantilever and b) simply supported beams when exposed to a varying electric field

First of all, the reader shall take into account that the results obtained for the beam made with AS4/epoxy laminae cannot be compared to the ones for the E-Glass fibers since both beams have different dimensions as it is specified in Figure 4.2.2. However they can be used to compare the distinct responses achieved for different beam stiffness.

In Figure 4.3.1a, the displacements of two cantilever beams made of both laminae materials proposed, AS4/epoxy and E-Glass/epoxy, are shown when they are subjected to different values of an external electric field. One can see that in both materials the maximum vertical displacement decreases almost linearly as more electric field is applied to the beam. Due to their different material properties and thickness, the displacements observed are different for any value of the electric field.

The beam made of E-Glass fibers is subjected to lower displacement as it could have been expected by looking at their corresponding stiffness ($5.258\ 10^4\ Nm^2$ and $2.051\ 10^4\ Nm^2$ for E-Glass/epoxy and AS4/epoxy laminae respectively). Beam made of E-Glass fibers is more than 2 times stiffer than the one made with AS4/epoxy fibers due to the contribution to the moment of inertia of the higher thickness of E-Glass/epoxy laminae, even though the longitudinal stiffness of AS4/epoxy laminae is higher than the one of E-Glass/epoxy.

Figure 4.3.1b shows the vertical displacement for the same beams with simply supported boundary conditions. A change in the beam response to the electric

field is appreciated. In this case the application of an increasing electric field contributes to an increment of the maximum displacement. In addition, the maximum displacements are observed to be lower than in the case of the cantilever beams. The reader should recall that negative displacements stand for downward displacements.

However, when focusing on the change of displacement in terms of percentage for the maximum electric field with respect to the situation of null electric field, which is expressed in Figure 4.3.2. The analyzed cantilever beams exhibit a decrease of -30.05% and -41.78% with respect to the null case for E-Glass/epoxy and AS4/epoxy laminae respectively when they are subjected to the maximum considered electric field (350 kV/m) and 100.5% and 72.3% for simply supported beams. Therefore although there is lower displacement in the simply support condition, greater variations in the beam movements than in the clamped case can be achieved through the piezoelectric effect.

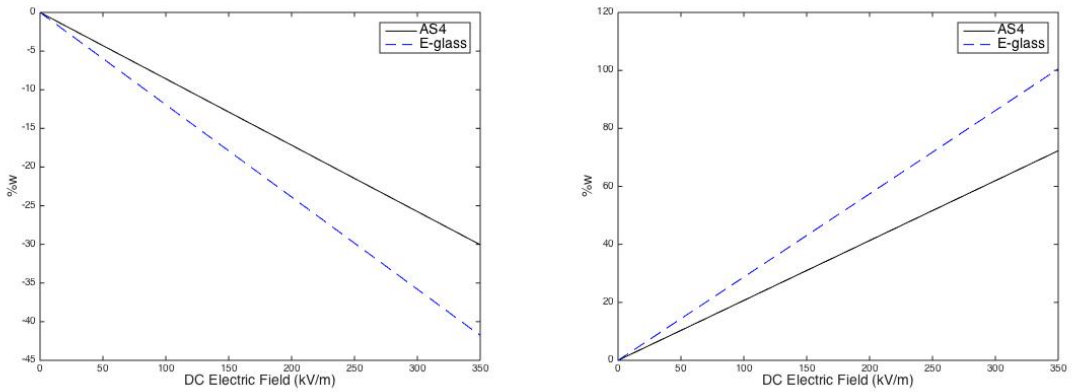

(a) (b)

Figure 4.3.2: Change in vertical displacement for $[90/0/p/90/0/p]_{4S}$ laminate in a) cantilever and b) simply supported beams when exposed to a varying electric field

Additionally, the obtained rotations are seen in Figure 4.3.3 and 4.3.4, which show the same behavior as the one followed by their corresponding displacements under the presence of a varying electric field. The rotations observed in the simply supported beams are lower than in the cantilever beams while the change in rotations are higher. A maximum rotation of -43.59% for E-Glass and -33.76% for AS4/epoxy is achieved in the clamped boundary condition. For the simply support case these changes are found to be higher, 125.3% and 90.16% for E-Glass and AS4/epoxy respectively.

Two interesting aspects arise out of this first study which are worthy to be mentioned: the difference observed between both laminate materials and the dissimilarities in the response to the electric field depending on the boundary condition applied.

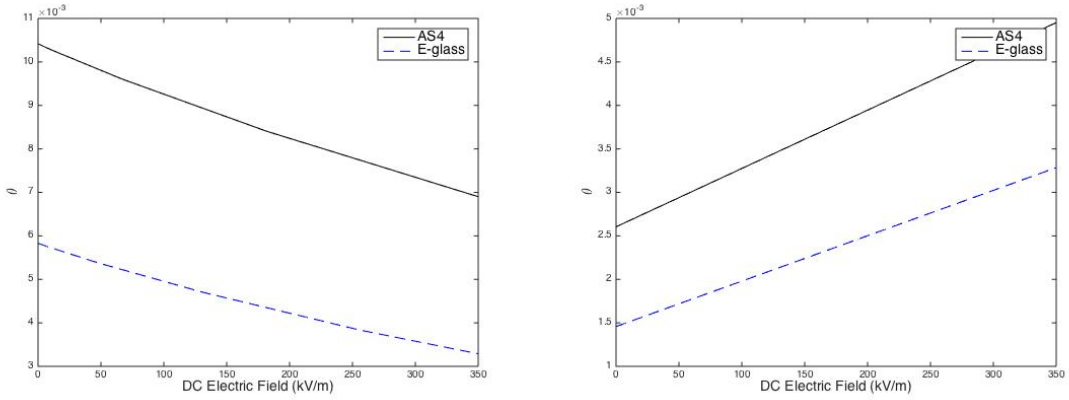

(a) (b)

Figure 4.3.3: Rotation for $[90/0/\mathrm{p}/90/0/\mathrm{p}]_{4S}$ laminate in a) cantilever and b) simply supported beams when exposed to a varying electric field

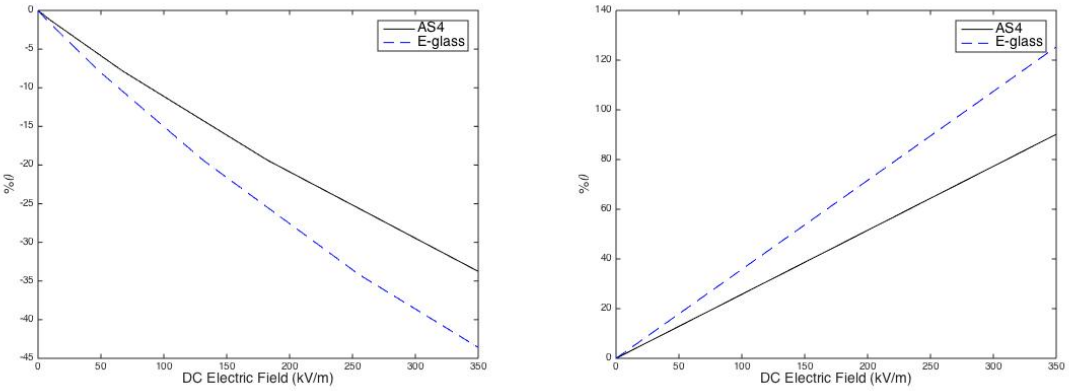

(a) Rotation for cantilever beam (b) Rotation for simply supported beam

Figure 4.3.4: Change in rotation for $[90/0/\mathrm{p}/90/0/\mathrm{p}]_{4S}$ laminate in a) cantilever and b) simply supported beams when exposed to a varying electric field

On one hand, the fact that the change in displacement for any applied electric field with respect to null electric field is different depending on the material used for the laminae, although the change of displacement due to the applied voltage only depends on the piezoelectric material. This dissimilarity comes from the different laminae thickness , which leads to different piezoelectric matrix terms H_{ij} (3.30) and therefore different reactions when the beams are subjected to an external electric field. If the comparison is made with different materials with the same thickness, although different displacement will be obtained, the relative change in displacement produced by the electric field will be the same.

On the other hand, the distinct responses of the beams to an increasing electric field between both boundary conditions are shown in two different ways. There is a change in the direction of the movement relative to the null electric field

state, which implies for instance an increase in the vertical displacement for simply supported beams while an alleviation of it for cantilever beams. The other difference is demonstrated by the difference between both cases in the values of displacements and rotations at any electric field, including the null electric field case.

First of all, the change in the direction of the movement between both boundary conditions produced by the electric field comes from the boundary condition constants c_1, c_2, c_3 and c_4. While boundary condition constants of the clamped case only depend on the applied load, the simply supported constant c_3 depends on the electric field, $c_3 = \left[\alpha_{xx}T_1 + D_{11}^*(D_{12}\alpha_{yy}T_1 + 2D_{16}\alpha_{xy}T_1 + E_{z(1)}^P H_{16})\right]\frac{L}{2} + \frac{q_0 bL^3}{24EI}$. When applied to the displacement and rotation expressions (4.10) and (4.11), it introduces a contribution of greater value and opposite sign to the part of the expressions which depend on the electric field before applying boundary condition.

Afterwards, the dissimilarity in the values obtained for both conditions is compared with the theoretical maximum vertical displacement and rotation, which are given by 4.22 and 4.23 respectively, being the corresponding coefficients for each case expressed in Table 4.3.1.

$$w = \frac{qL^4}{\alpha EI} \tag{4.22}$$

$$\theta = \frac{qL^3}{\beta EI} \tag{4.23}$$

	α	β
cantilever beam	8	6
simply supported beam	$\frac{384}{5}$	24

Table 4.3.1: Values of the theoretical maximum displacement constants for clamped and simply supported conditions

Lower rotations and vertical displacements have been found in the results for simply supported beams, which agrees with the theoretical maximum movements of these boundary conditions, given by the values of the coefficients α and β in Table 4.3.1. Nevertheless, more relative changes in the movements with respect to the case of null electric field have been obtained for the simply supported condition since the variation in movement generated by the electric field is referred to a lower value.

4.3.2 Temperature variation

Similar to what was analyzed with the study accomplished in the previous section of a beam made of two different laminae materials and boundary conditions

exposed to an external electric field, the beam is going to be subjected now to a temperature difference along the thickness direction in order to assess how it affects its displacement and rotation. The temperature difference is produced by distinct temperature at the upper end of the beam and at the bottom side.

Nevertheless from this section on, only results of the percentage of variation in the movements' magnitudes with respect to the reference case (either null electric field or null temperature difference) are going to be expressed since the are the key parameters so as to analyze the capacity of control over deflections.

When subjected to a varying temperature difference, the beam shows a linear change of movements with respect to the temperature difference. The analysis is accomplished considering a positive temperature difference Whenever there is higher temperature at the top end than at the bottom. The positive temperature gradient produces higher thermal expansion in the top laminate than in the lower one, resulting in an opposite effect for negative temperature gradients. For the cantilever beam case, it is observed that a positive temperature difference, i.e. higher temperature at the top end than at the bottom, enlarges the maximum rotation and downward displacement.

Furthermore, it is also appreciated that the beam made of E-Glass/epoxy laminae is more sensitive to a temperature difference between both beam sides. There is a dissimilarity in the longitudinal thermal coefficient α_1, since the α_1 for E-Glass/epoxy laminae is positive and higher than the one of AS4/epoxy material, as seen in Table 4.2.1. However, since beam made of E-Glass fiber is thicker, the temperature difference per unit meter is lower for E-Glass beam than the one for AS4/epoxy laminates. Therefore, this dissimilarity in the thermal coefficient has been found to imply a greater effect over the temperature sensitivity than the difference in the beam thickness.

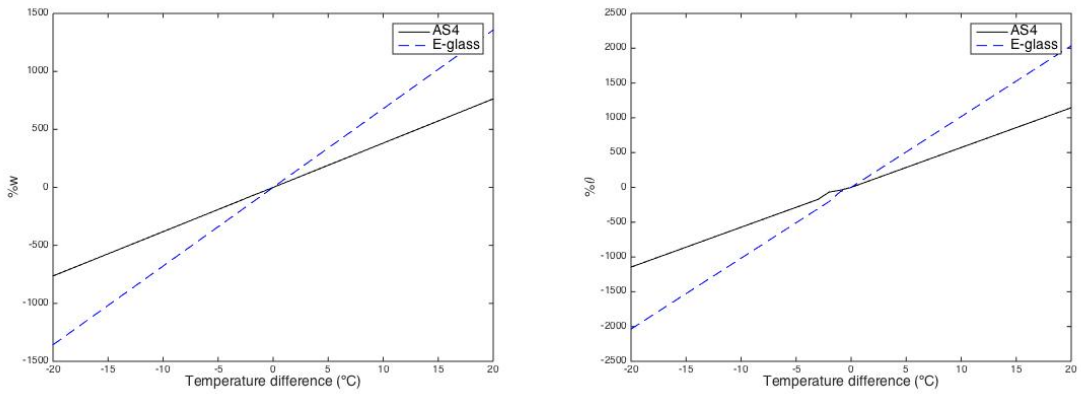

(a) (b)

Figure 4.3.5: Change in a) vertical displacement and b) rotation for $[90/0/p/90/0/p]_{4S}$ laminate in cantilever beams when exposed to a varying temperature difference

Regarding the simply supported beams, Figure 4.3.6, they show the same features in the comparison with cantilever beams than when they were exposed to electric field: there is a change in the direction of the movement if compared to cantilever beams and they experience again even more relative displacements and rotations than in the clamped case.

One can observe that the change in displacements and rotations obtained are much higher than the ones obtained for the exposure to electric field. However the 20ºC temperature difference selected is a very high difference for such thin beams. This huge temperature gradient exhibited in few centimeters could be an extreme situation in which the beam might be subjected to ambient conditions at one of its sides. Additionally the electric field at which the beam can be exposed could have been increased to the maximum that the PZT-5H can withstand ($500\,kV/m$).

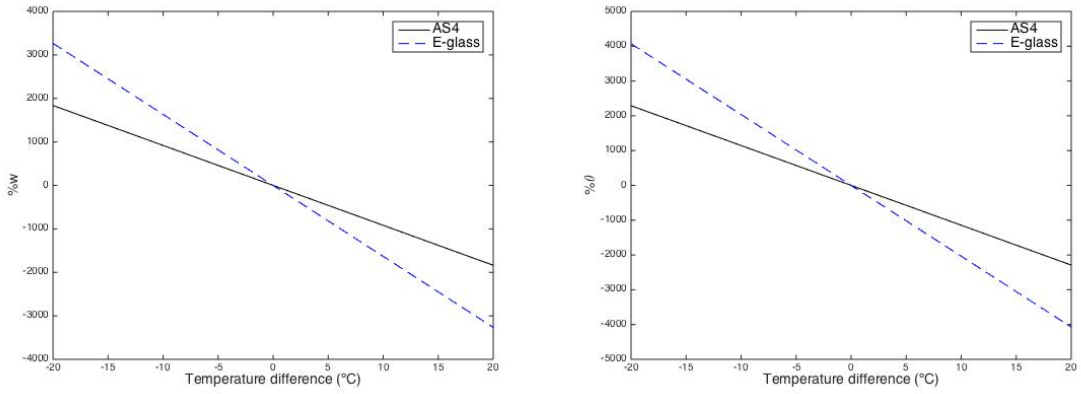

(a) (b)

Figure 4.3.6: Change in a) vertical displacement and b) rotation for $[90/0/\mathrm{p}/90/0/\mathrm{p}]_{4S}$ laminate in simply supported beams when exposed to a varying temperature difference

CHAPTER 5

Result analysis

5.1 Introduction

Previous chapter was devoted to apply the theoretical model to two practical beam examples and assess how temperature difference and electric field exposures modify the beam deflections, which can be used in order to explore the chances to modify the beam behavior.

This chapter deals with the analysis of the results previously obtained. First of all different stacking sequences are going to be studied by changing the order of laminae while keeping the total number of layers and the number of layers of each material and orientation in order to enable a comparison of the beam sensibility to temperature and electric field depending on the stacking sequence selected.

The stacking sequences to be analyzed are:
- sequence 1: $[0/90/\mathrm{p}/0/90/\mathrm{p}]_{4S}$
- sequence 2: $[\mathrm{p}/0/90/\mathrm{p}/0/90]_{4S}$
- sequence 3: $[90/0/\mathrm{p}/90/0/\mathrm{p}]_{4S}$
- sequence 4: $[\mathrm{p}/90/0/\mathrm{p}/90/0]_{4S}$
- sequence 5: $[p_2/0_2/90_2]_{4S}$
- sequence 6: $[p_2/90_2/0_2]_{4S}$
- sequence 7: $[90_2/0_2/p_2]_{4S}$
- sequence 8: $[90_2/p_2/0_2]_{4S}$

being p the layer corresponding to the piezoelectric material.

Thereafter, the stacking sequence which turns to be more easily controllable when exposed to an electric field will be analyzed to see how the thickness of two beam components affect the beam behavior. Firstly, the core thickness will be varied in order to study how the core thickness selection will impact on the beam movements. Afterwards, the piezoelectric thickness will also be varied by adding several piezoelectric layers stuck together, for instance: $[0/90/p_n/0/90/p_n]_{4S}$ where n is the parameter related to the number of piezoelectric materials attached together.

Lately, this most controllable stacking sequence will also be studied, subjecting

it to the simultaneous presence of temperature and electric field perturbations. In order to do so, two different studies are performed: the effect of the exposure to some range of temperature difference while being in presence of some reasonable electric field values and the other way round.

5.2 Analysis of stacking sequences

Once the effects produced by the electric field and the temperature difference have been analyzed in a $[90/0/p/90/0/p]_{4S}$ laminae beam, it is time to focus on how these two effects will vary when using other stacking sequence.

The corresponding stiffness of each of the laminate materials are described in Table 5.2.1. Since the same number of each type of laminae than in the sequence used in section 4.3 is conserved in all the sequences, the beam geometries are the same as the ones defined in Figure 4.2.2.

Laminate	Seq. 1	Seq. 2	Seq. 3	Seq. 4	Seq. 5	Seq. 6	Seq. 7	Seq. 8
AS4	2.064	2.658	2.051	2.645	2.664	2.638	2.641	2.608
E-Glass	5.281	6.801	5.258	6.777	6.846	6.800	6.664	6.702

Table 5.2.1: Stiffness for each of the laminate sequence, measured in $Nm^2 \cdot 10^4$

5.2.1 Voltage variation

Figure 5.2.1 shows the variation in displacement of all the analyzed sequences for an increasing positive voltage gradient for the AS4/epoxy laminate beam. Changes in movements with voltage are seen to be nearly linear. Two different groups are observed. The first group is the one with lower relative movement and it corresponds to *sequence 1* and *sequence 3*, which are the sequences of lower stiffness. The rest of the sequences show a common behavior among them while they have a similar stiffness. These two different groups are clearly seen in Figure 5.2.2, in which the change in the maximum vertical displacement is related to the corresponding stiffness of each of the stacking sequences. It is appreciated that there is not a linear relation between stacking sequence stiffness and beam deflections although they are highly related.

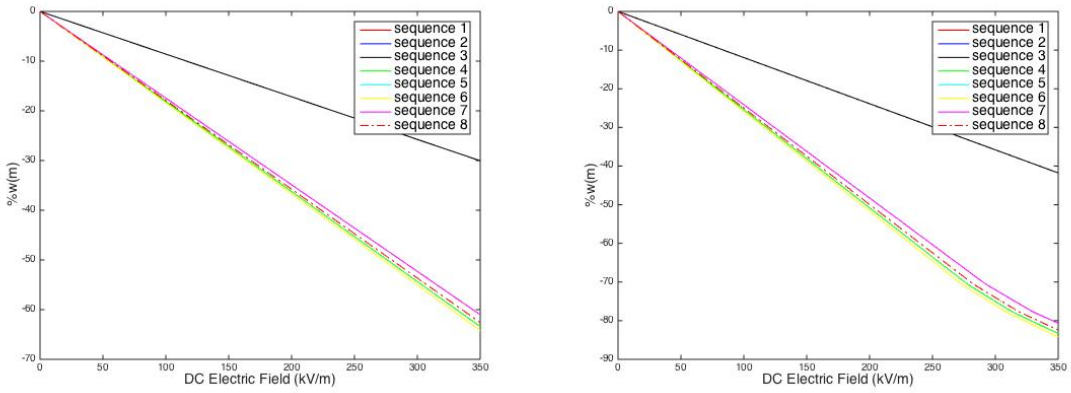

(a) (b)

Figure 5.2.1: Maximum change in vertical displacement for several stacking sequences for cantilever beams with a) AS4/epoxy fibers and b) E-Glass fibers when subjected to a variable electric field

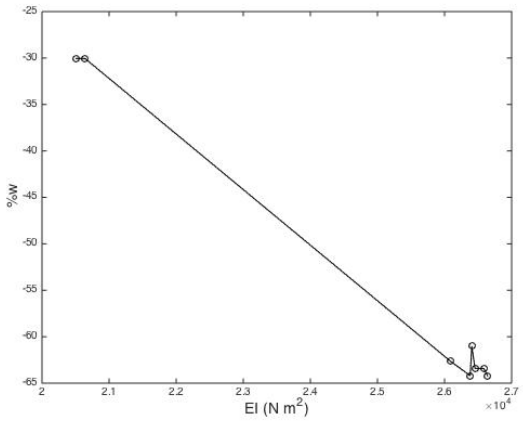

Figure 5.2.2: Change in maximum vertical displacement for each of the selected stacking sequences as a function of their stiffness

Now that it seems clear the importance of the beam stiffness in the resulting relative movement, it might be interesting to search for the reason behind the stiffness difference. The sequences with higher stiffness are the ones whose stacking sequences start by a piezoelectric layer, being the one with the highest stiffness *sequence 5*, which starts by two consecutive layers of piezoelectric material.

The worst sequence in order to build a stiff beam is found to be those sequences which begins with a 90º fiber lamina, followed by a 0º one and by the PZT-5H, as it occurs in *sequence 3*. However if two of each are stuck consecutively, as in *sequence 7*, the resulting beam is even stiffer.

Sequence 5 is also the sequence whose relative movement is more affected by the electric field. The reason is found in the piezoelectric matrix H_{ij}. As it is seen in (3.30), H_{ij} depends on the height of the piezoelectric layer, being increased

its value the greater the distance of the piezoelectric layers to the middle plane. The value of the piezoelectric matrix will affect the final beam movements when exposed to electric field.

Therefore it could be concluded that there are two key factors which are highly related with the relative displacement for a given applied electric field with respect to null electric field as a percentage: the beam stiffness and the location of the piezoelectric material in the stacking sequence. Additionally, placing below the piezoelectric material fibers at 0^o rather than at 90^o, increases slightly the percentage of change in the beam movements.

For the sake of clarity for the reader and in order to avoid an excessive number of figures, the rest of cases are going to be analyzed focusing only in the maximum relative displacements and rotations corresponding to the exposure to 350 kV/m with respect to the situation of null electric field.

Figure 5.2.4 shows the maximum variations in rotation for the cantilever beams. Highest rotation gains are observed in the same sequences where they were developed in the case of the displacements.

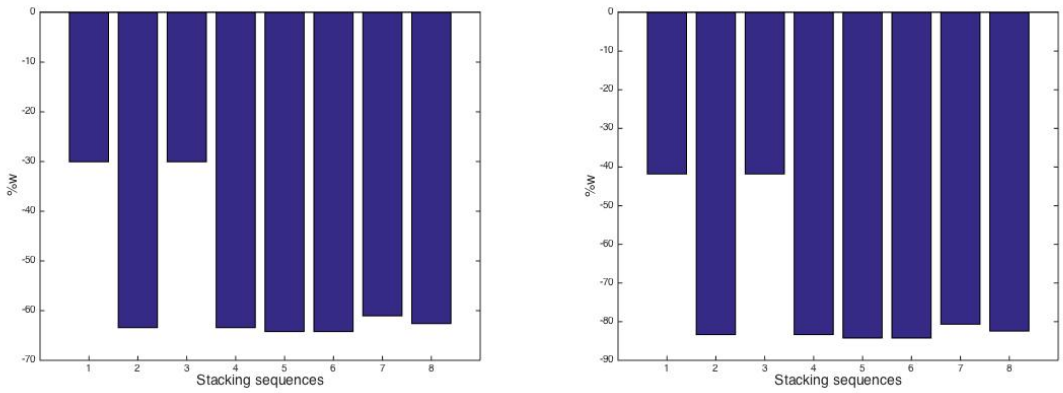

(a) (b)

Figure 5.2.3: Change in maximum vertical displacement of the studied stacking sequences for cantilever beams with a) AS4/epoxy laminae and b) E-Glass/epoxy laminae when subjected to 350 kV/m electric field.

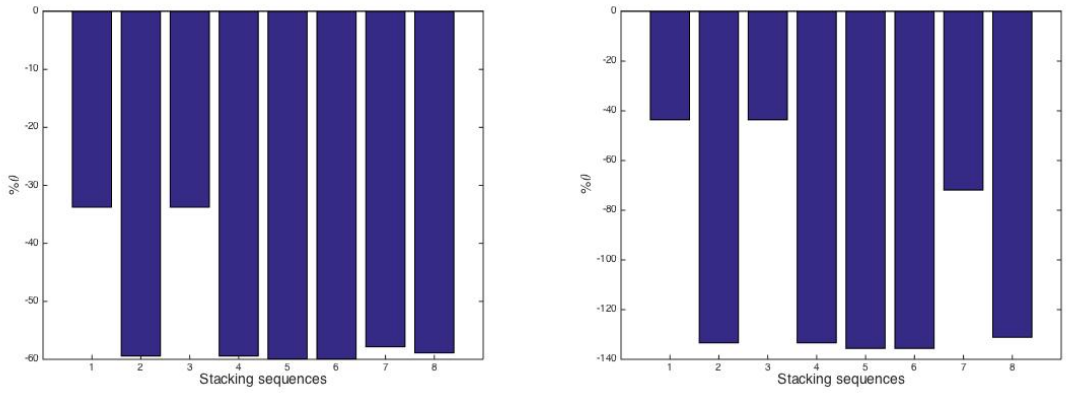

(a) (b)

Figure 5.2.4: Change in maximum rotation of the studied stacking sequences for cantilever beams with a) AS4/epoxy laminae and b) E-Glass/epoxy laminae when subjected to 350 kV/m electric field.

Regarding the simply supported beams, the maximum displacements and rotations are also produced in those same stacking sequences but with the opposite direction as the ones originated in the cantilever beams due to the distinct contributions in the beam movements produced in each of the boundary conditions, as it was mentioned in the previous chapter with the analysis of *sequence 3*.

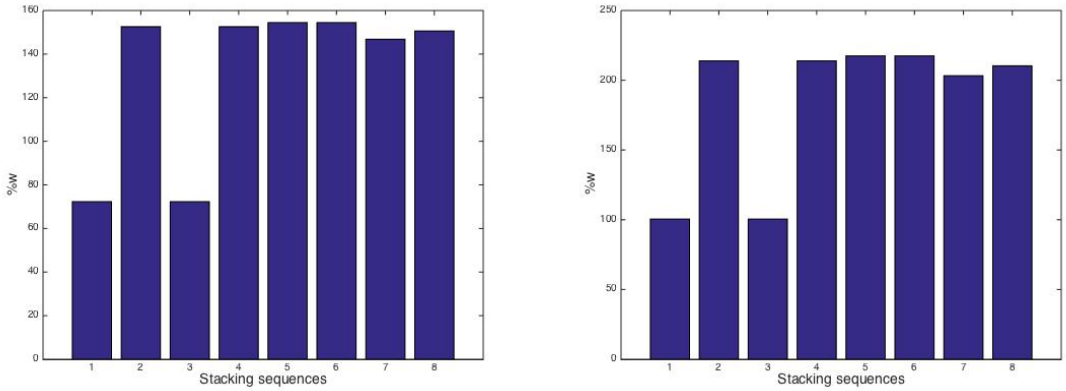

(a) (b)

Figure 5.2.5: Change in maximum vertical displacement of the studied stacking sequences for simply supported beams with a) AS4/epoxy laminae and b) E-Glass/epoxy laminae when subjected to 350 kV/m electric field.

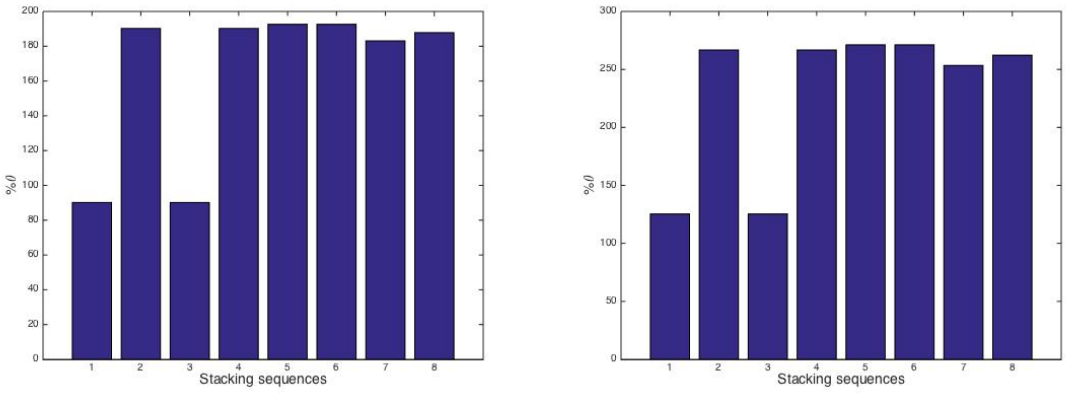

(a) (b)

Figure 5.2.6: Change in maximum rotation of the studied stacking sequences for simply supported beams with a) AS4/epoxy laminae and b) E-Glass/epoxy laminae when subjected to 350 kV/m electric field.

5.2.2 Temperature variation

The impact on the beam movements of the stacking sequences selection for a beam subjected to a temperature gradient is analyzed in this section. To do this study, the beams have being exposed to a temperature where there is 5°C more at the top end of the beam than at the bottom one. Any other temperature difference can be deduced since there exists a linear relation between any temperature difference and the case of no temperature difference, as it was explained in the section 4.3.2. Moreover, whenever there is a negative temperature difference, i.e. higher temperature at the bottom than at the top, the variations in movements will be the same as the one which would be produced by the corresponding positive temperature difference with the opposite direction.

Those stacking sequences starting by a piezoelectric layer are found to show less relative displacement and rotation. This behavior is boosted slightly if two consecutive piezoelectric layers are placed at the beginning of the stacking sequence. It is also known that a 90° laminae at the top of the stacking sequence contributes to higher variations in movements due to temperature gradients. So it is concluded that in order to increase the relative displacement produced by a temperature difference, it is advisable to accumulate 90° layers at the beginning of the stacking sequence, followed by 0° orientation fibers and finishing with the piezoelectric layers.

The reason behind this sensitivity to the stacking sequence selected regarding the beam response to a temperature gradient is found in the dissimilarity in the thermal expansion coefficients between the materials used. As seen in Table 4.2.1, both of the material fibers have higher thermal coefficient in the transverse direction (90^o) than in longitudinal direction (0^o).

Consequently, the most suitable stacking sequence to achieve a beam with the

highest movement variation due to exposure to a temperature difference is found to be, for both studied materials, the one which concentrates 90º laminae at the top of the sequence and ends with the piezoelectric material, with 0º laminae between both. This suitable stacking sequence for temperature gradients is the one with the lowest variation of movements due to an electric field presence among the studied sequences.

Figures 5.2.7 and 5.2.8 show the change in vertical displacement and rotation exhibited by the beams when they are exposed to the selected temperature gradient. The difference in the thermal expansion coefficients produces that the variations in the beam movements are enhanced in those beams with E-Glass/epoxy laminae, due to its higher longitudinal and transverse thermal expansion coefficient.

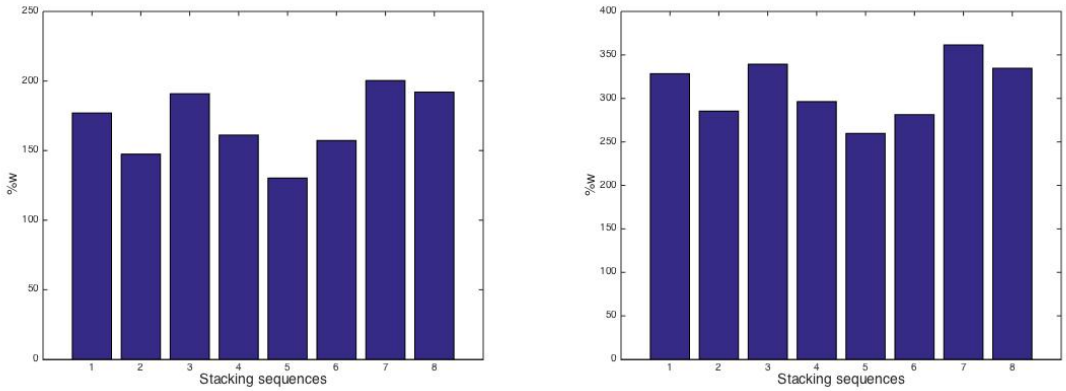

(a) (b)

Figure 5.2.7: Change in maximum vertical displacement of the studied stacking sequences for cantilever beams with a) AS4/epoxy laminae and b) E-Glass/epoxy laminae when subjected to 5ºC temperature difference between the top and bottom beam surfaces

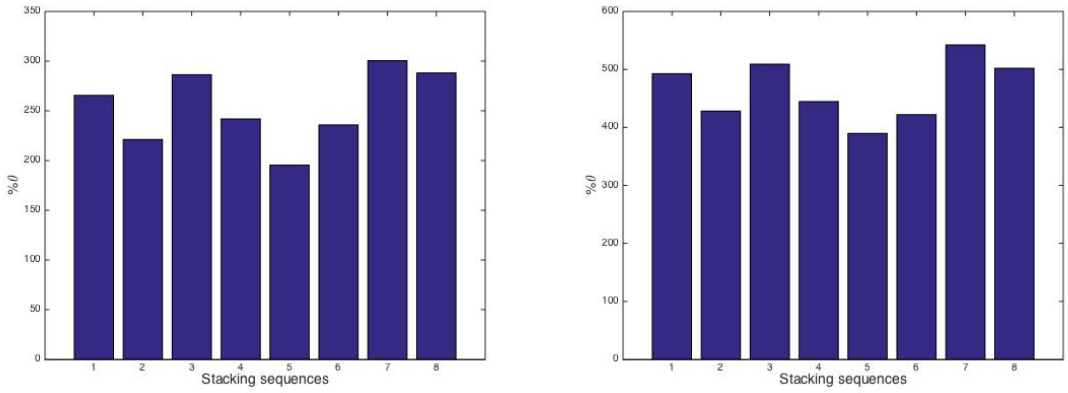

(a) (b)

Figure 5.2.8: Change in maximum rotation of the studied stacking sequences for cantilever beams with a) AS4/epoxy laminae and b) E-Glass/epoxy laminae when subjected to 5ºC temperature difference between the top and bottom beam surfaces

Furthermore, by analyzing the results indicated in Figures 5.2.9 and 5.2.10 for simply supported beams, one can realize that the variations in the movements produced by the temperature gradient are higher in absolute term than the one obtained for the clamped situation with opposite direction, as it occurred to happen in the rest of the studies.

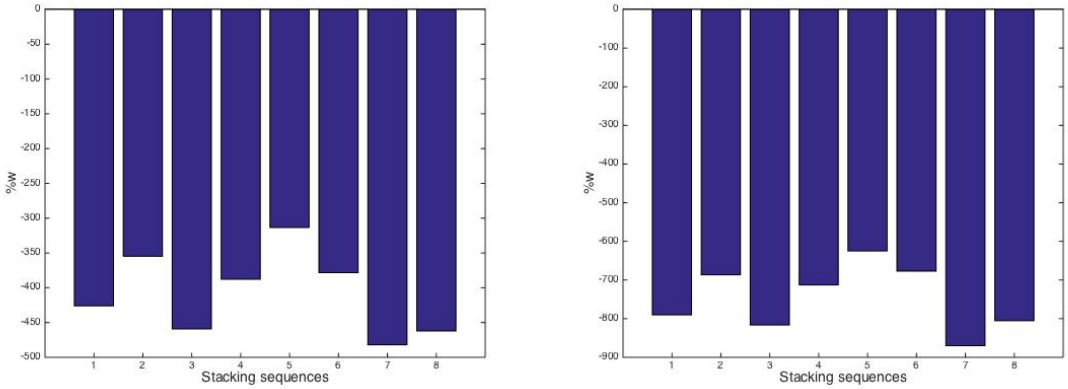

(a) (b)

Figure 5.2.9: Change in maximum vertical displacement of the studied stacking sequences for simply supported beams with a) AS4/epoxy laminae and b) E-Glass/epoxy laminae when subjected to 5ºC temperature difference between the top and bottom beam surfaces

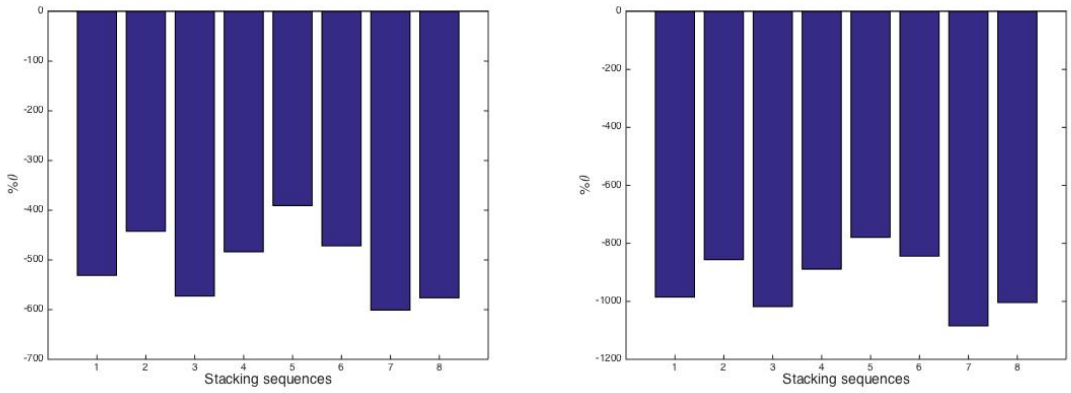

(a) (b)

Figure 5.2.10: Change in maximum rotation of the studied stacking sequences for simply supported beams with a) AS4/epoxy laminae and b) E-Glass/epoxy laminae when subjected to 5°C temperature difference between the top and bottom beam surfaces

5.3 Core thickness sensitivity

One of the goals of previous section was to analyze relative movements of several stacking sequences to see which one would be the most suitable in order to enable a control in the movement generated by a given load. The conclusion obtained is that *sequence 5* is the one with the most movement control capability within the studied sequences when subjected to an electric field due to its high stiffness and the position of the piezoelectric materials, as it can be appreciated in Figure 5.2.3, Figure 5.2.4, Figure 5.2.5 and Figure 5.2.6.

Once the laminate sequences have been analyzed, the effect of using different core thickness is desired to be studied in order to see how it affects the maximum variation in movement which can be achieved with respect to the case when there is no temperature and voltage difference. The study is going to be performed with *sequence 5* due to its possibility to obtain high control capability under an electric field, which is the one of the main goals of this dissertation.

To asses the influence of the core thickness, a range of eight different values have been selected depending on the laminate material, since the core thickness t_c has been set to be four times higher than the sum of the thickness produced by both the top and bottom stacking sequences, t_l: $0.25t_c$, $0.5t_c$, $0.75t_c$, t_c, $1.25t_c$, $1.5t_c$, $1.75t_c$ and $2t_c$.

Similarly to what it was done in previous sections, the core thickness assessment will be split into two, analyzing separately the movement variations obtained

between the situation with no external influence and the exposure to a 350 kV/m electric field and to 5ºC temperature difference between the top and bottom beam surfaces.

Figure 5.3.1 shows the maximum vertical displacement and rotation of a cantilever beam with variable core thickness when there is 5ºC temperature gradient between the top and bottom beam surfaces. First of all, when focusing on how the core thickness affects the variations in movements in each of the beams, a similar behavior of the beam response is observed. However there is a slight difference as the core becomes thicker and thicker. The fact that beams made of E-Glass/epoxy laminae reach higher values of core thickness is connected to the relation established between core and laminae thickness, with E-Glass/epoxy laminae being thicker than AS4/epoxy.

For cantilever beams an increase in the beam core thickness produces higher variations in the beam deflections. This movement enlargement is caused by the greater distance from the laminae to the beam symmetry axis, which increase D and H matrices as seen in (3.29) and (3.30), enhancing vertical displacements and rotations in the beams as it is expressed in (4.10) and (4.11).

Notice that the relation obtained between the core thickness and the beam movement is not linear but parabolic. Dashed lines are the resulting linear regression of the eight different values for the core thickness in each of the beams. For cantilever beams the four middle values among the selected ones for the core thickness are found to lie below the linear regression line, which implies that any of these values of core thickness lead to less deflection than the one that would have led if a linear relationship were established between core thickness and beam movements. This parabolic behavior can be interested for a tradeoff study regarding movement sensitivity to electric field versus weight.

As in the rest of the studies, simply supported beams show also a similar behavior than cantilever beams but with movements in the opposite directions for the core thickness study.

When the beams are subjected to the 350 kV/m electric field, analogous behavior for the beams is observed. The main difference is seen in the maximum rotation for cantilever beams, Figure 5.3.3b, where the parabolic is found not to be so smooth. However, even in this case the coefficient of determination R^2 still indicates a good linear approximation: $R^2 = 0.936$.

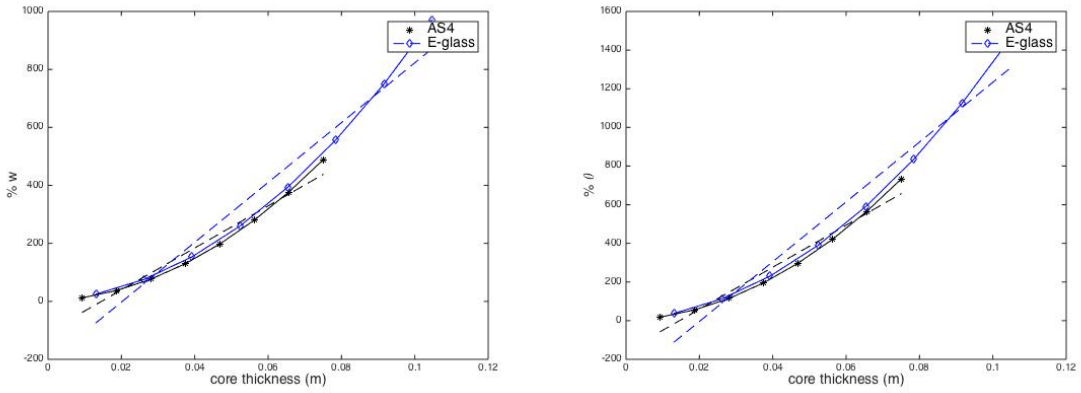

(a) (b)

Figure 5.3.1: Change in maximum a) vertical displacement and b) rotation for AS4/epoxy and E-Glass/epoxy laminae in cantilever beams for different values of the core thickness when subjected to 5ºC more at the top than at bottom beam surface.

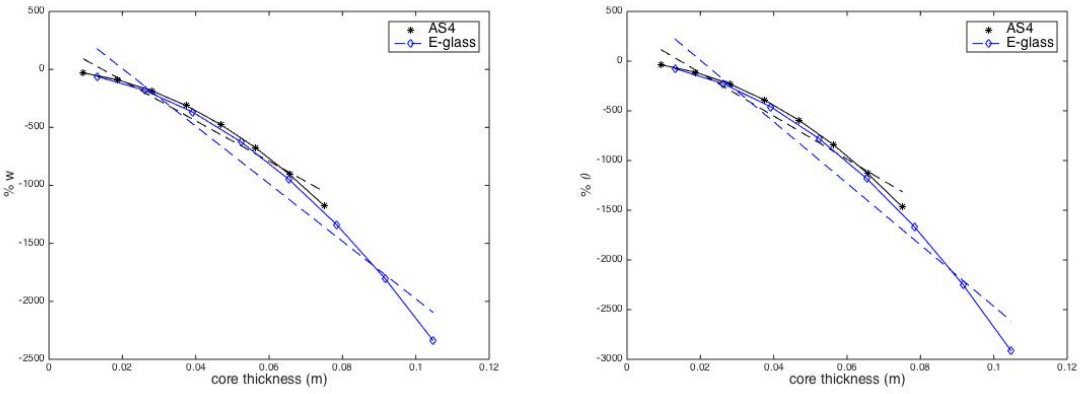

(a) (b)

Figure 5.3.2: Change in maximum a) vertical displacement and b) rotation for AS4/epoxy and E-Glass/epoxy laminae in simply supported beams for different values of the core thickness when subjected to 5ºC more at the top than at bottom beam surface.

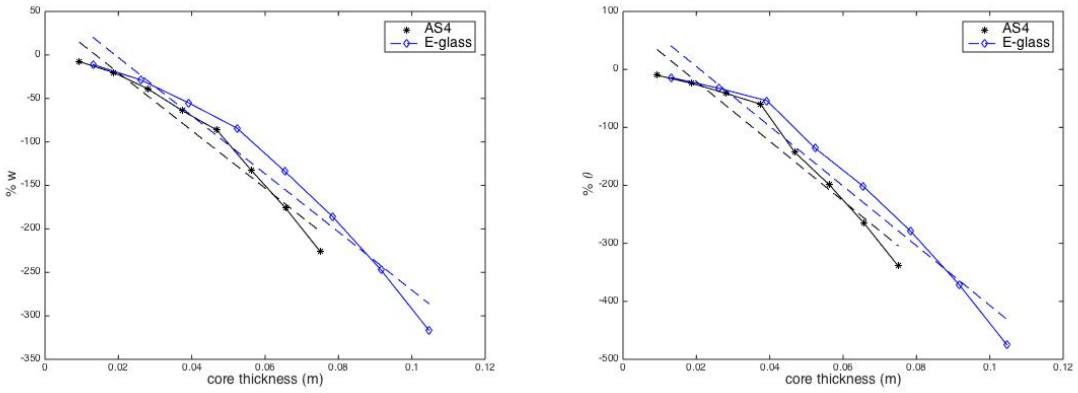

(a) (b)

Figure 5.3.3: Change in maximum a) vertical displacement and b) rotation for AS4/epoxy and E-Glass/epoxy laminae in cantilever beams for different values of the core thickness when subjected to 350 kV/m electric field.

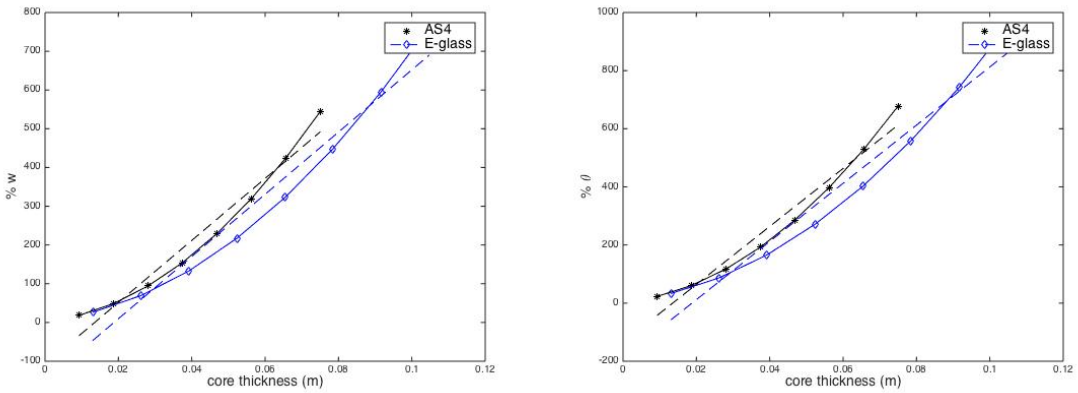

(a) (b)

Figure 5.3.4: Change in maximum a) vertical displacement and b) rotation for AS4/epoxy and E-Glass/epoxy laminae in simply supported beams for different values of the core thickness when subjected to 350 kV/m electric field.

5.4 Piezoelectric layers sensitivity

The assessment of the effect produce by the accumulation of several piezoelectric layers bonded together is analyzed in this section. The stacking sequence selected for that purpose is again the one with most movement control capability, which has been found to be $[p_2/0_2/90_2]_{4S}$, to assess how much the maximum variations in movements can be increased with respect to their corresponding movements at null electric field. The addition of several layers tightened together implies basically the same effect than increasing the piezoelectric layer thickness. The stacking sequences analyzed are based on *Sequence 5*, increasing the number of piezoelectric materials $[p_n/0_2/90_2]_{4S}$, with n going from 2 to 5.

As expected, the more piezoelectric layers are used, the higher variations in movements are observed when the beams are exposed to an electric field. Figure 5.4.1, Figure 5.4.2, Figure 5.4.3 and Figure 5.4.4 show the maximum relative movements produced when the electric field has reached the selected value (*350 kV/m*). The dashed lines of the figures are the representations of the linear regressions of the respective curves. The relation of the variation in movement with the number of piezoelectric material layers are not linear but very close to it, approaching the coefficient of determination of the linear regression to one in all of them. The maximum variation of the displacement and rotation obtained for $[p_5/0_2/90_2]_{4S}$ with respect to $[p_2/0_2/90_2]_{4S}$ are found to be enhanced up to the values shown in Table 5.4.1.

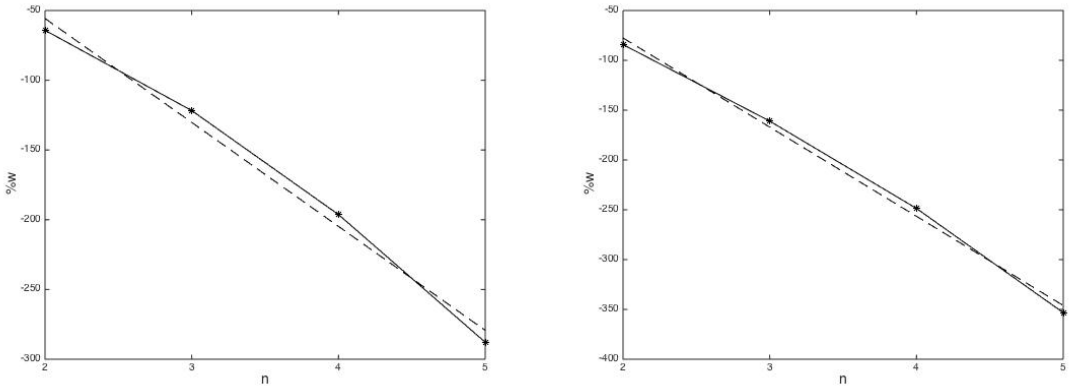

(a) (b)

Figure 5.4.1: Change in maximum vertical displacement for n piezoelectric layers for cantilever beams with a) AS4/epoxy laminae and b) E-Glass/epoxy laminae, when subjected to 350 kV/m electric field

	Clamped AS4/epoxy laminae	Clamped E-Glass/epoxy laminae	Simply supported AS4/epoxy laminae	Simply supported E-Glass/epoxy laminae
Displacement	287.8%	353.3%	692.5%	850%
Rotation	431.7%	529.9%	863.5%	1060%

Table 5.4.1: Maximum relative movements increment obtained for $[p_5/0_2/90_2]_{4S}$ with respect to $[p_2/0_2/90_2]_{4S}$

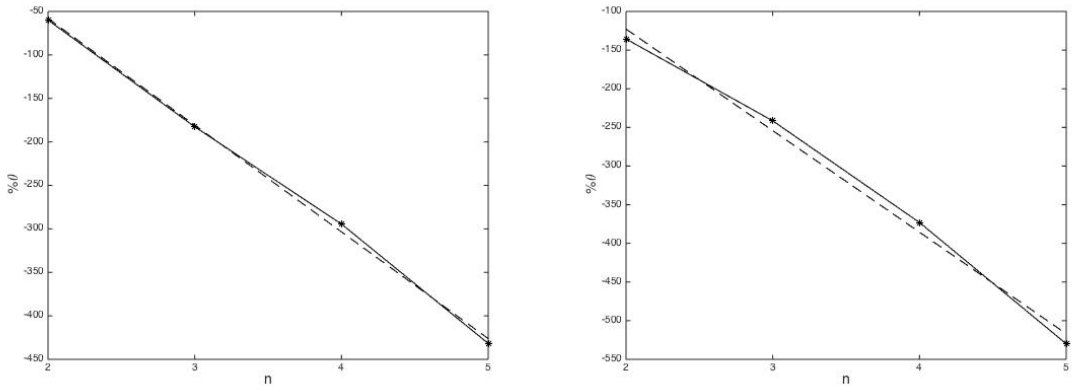

(a) (b)

Figure 5.4.2: Change in maximum rotation for n piezoelectric layers for cantilever beams a) AS4/epoxy laminae and b) E-Glass/epoxy laminae, when subjected to 350 kV/m electric field

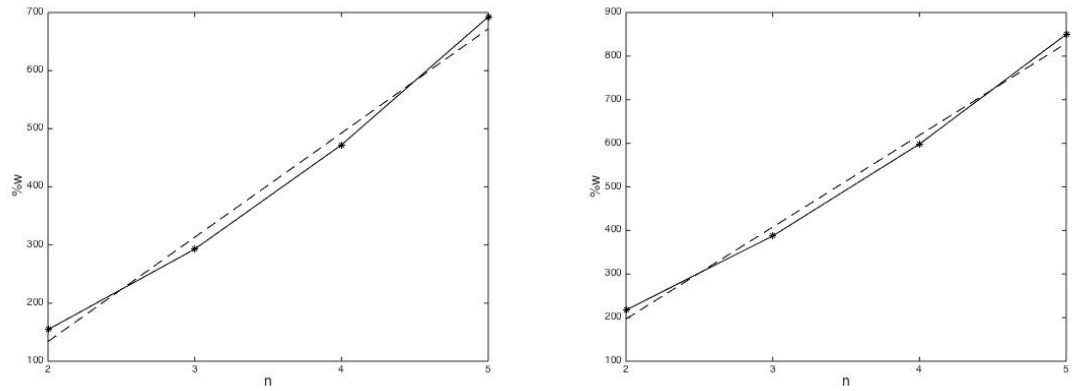

(a) (b)

Figure 5.4.3: Change in maximum displacement for n piezoelectric layers for simply supported beams a) AS4/epoxy laminae and b) E-Glass/epoxy laminae, when subjected to 350 kV/m electric field

Nevertheless, regarding the evolution of the movements for the increasing electric field, it appears a sudden variation in the slope at the vicinity of the value at which the beam deflections approach the double of the value exhibit for null electric field in the clamped case for AS4/epoxy fiber beam (Figure 5.4.5), recovering afterwards the initial slope. Meanwhile in the simply supported case this peak does not appear anymore, remaining the relation nearly linear for the whole electric field range (Figure 5.4.6). Since beams made of E-Glass/epoxy laminae present similar response to the increasing electric field, their figures have not been included to reduce the number of them. They also exhibit the sudden variation in slope for the clamped condition while no slope peak for the simply supported case.

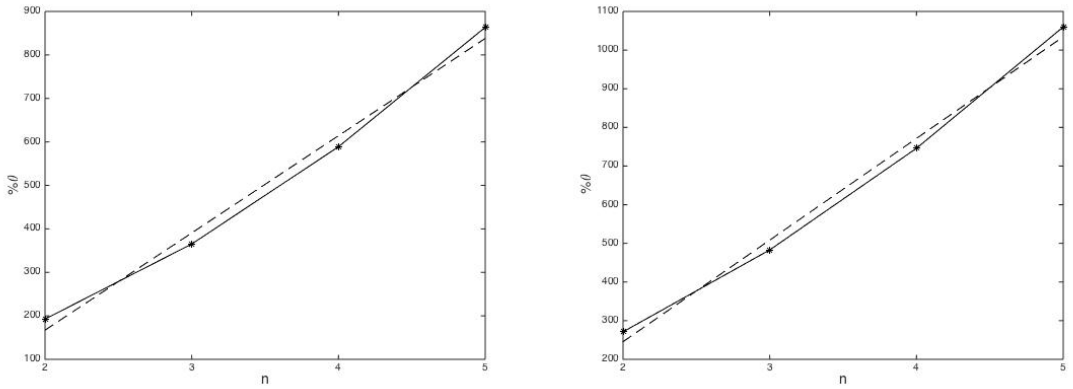

(a) (b)

Figure 5.4.4: Change in maximum rotation for n piezoelectric layers for simply supported beams a) AS4/epoxy laminae and b) E-Glass/epoxy laminae, when subjected to 350 kV/m electric field

As it can be observed, the appearance of the change of slope is delayed in those sequences with fewer number of piezoelectric layers. For the rotation of cantilever beams, Figure 5.4.5b, sequence with *n=2* has already started the change of slope but it has not completed it yet when the electric field reaches 350 KV/m. However in the vertical displacement of the cantilever beams, one can appreciate that the sequence with *n=3* has finished the change of slope. These discontinuities in the slope of the beam deflection imply that there is not a linear relation between the number of piezoelectric used and the variation in displacements and rotations obtained.

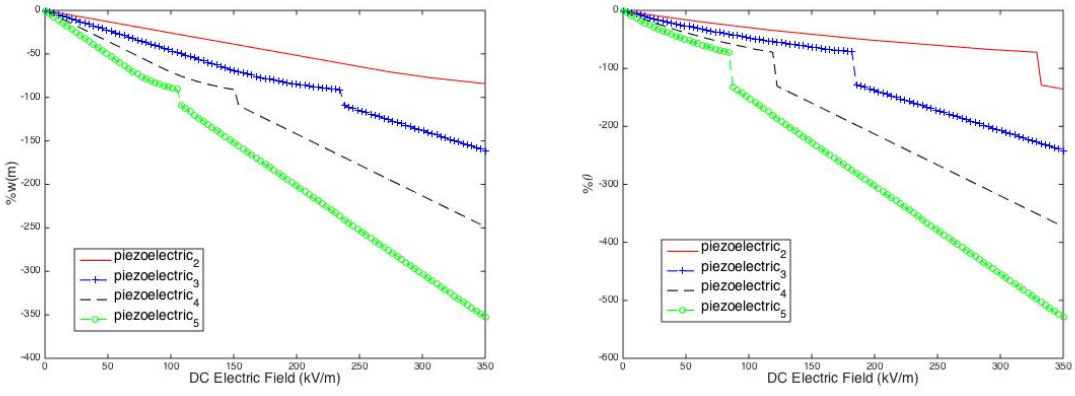

(a) (b)

Figure 5.4.5: Change in maximum a) vertical displacement and b) rotation of n piezoelectric layers for cantilever beams

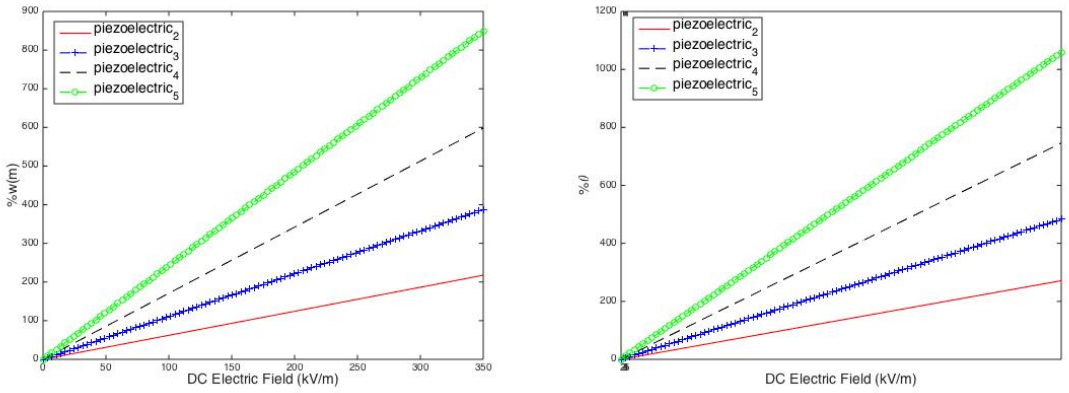

(a) (b)

Figure 5.4.6: Change in maximum a) vertical displacement and b) rotation of n piezoelectric layers for simply supported beams

5.5 Voltage and temperature simultaneous analysis

Static analyses to study the sensitivity of different stacking sequences to either an electric field or a temperature difference have been carried out in previous sections. The aim of this section is to perform the analysis of a beam with piezoelectric material within its sequence to see how it behaves under the influence of an electric field with a temperature difference along the beam thickness direction. Since the purpose of this dissertation is to obtain a beam with the biggest control over its deformation thanks to the piezoelectric material, *Sequence 5* has been chosen for this analysis due to the fact that it has shown the best capacity to change its movements over the sequences studied.

In order to assess the influence of both factors in the variation of the beam vertical displacements and rotations with respect to the case of null electric field and temperature difference, a study based on the effect of a change in temperature when the smart beam is subjected to certain electric field is accomplished.

By comparing the effect of a temperature difference on the beam movements from the case under null electric field to the one exposed to the maximum considered electric field, 350 kV/m, one can observe in Figure 5.5.1 that in cantilever beams there is a opposed contribution of the effects produced by a positive electric field and a positive temperature difference along the beam thickness direction, which leads to a reduction of variations of vertical displacement and rotation.

However for simply supported beams these contributions produce the opposite effect, generating an enhancement in the change in the beam deflections when such conditions occur, as it is seen in Figure 5.5.2. Beams made of E-Glass fibers exhibit the same behavior for the temperature difference sensitivity as the ones shown in Figures 5.5.1 and 5.5.2 for AS4/epoxy fibers but with different magnitudes.

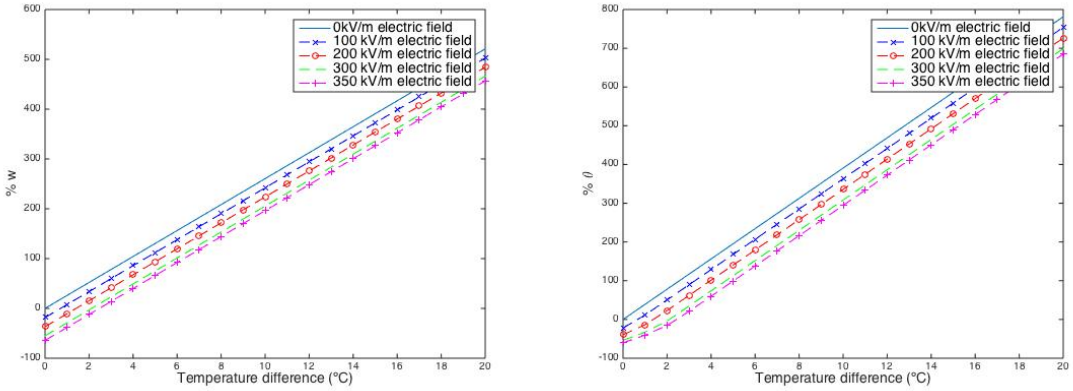

(a) (b)

Figure 5.5.1: Sensitivity of maximum variation in a) vertical displacement and b) rotation to temperature difference for cantilever beams with AS4/epoxy fiber.

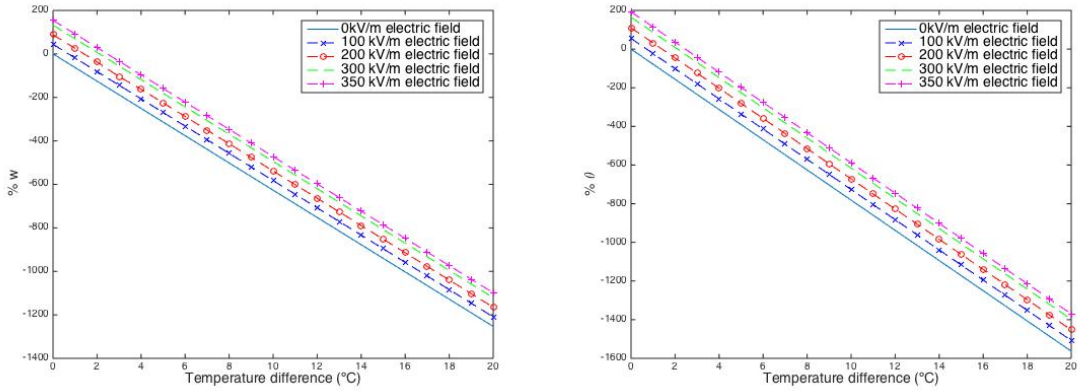

(a) (b)

Figure 5.5.2: Sensitivity of maximum variation in a) vertical displacement and b) rotation to temperature difference for simply supported beams with AS4/epoxy fiber.

For each electric field, the same linear relation is established, connecting beam movements with temperature difference. The variation in relative deflections produced by an unitary change in temperature is given by the slope of this relation, which is the same regardless of the magnitude of the electric field present. The slopes of the vertical displacements and rotations variations for both types of beams in the two different boundary conditions are detailed in Table 5.5.1. Furthermore, displacement and rotation slopes for simply supported beams are found to nearly duplicate the ones of cantilever beams due to the addition of both positive temperature and voltage gradients contributions. On the other hand, the intensity of the electric field determines only the intercepts of these curves.

	Vertical displacement	Rotation
Cantilever beam. AS4/epoxy fiber	26.05	39.07
Cantilever beam. E-Glass fiber	29.18	43.78
Simply supported beam. AS4/epoxy fiber	-62.67	-78.15
Simply supported beam. E-Glass fiber	-70.22	-87.55

Table 5.5.1: Different slopes for the vertical displacement and rotation variations versus temperature difference curves for a $[p_2/0_2/90_5]_{4S}$ cantilever and simply supported beam with AS4/epoxy or E-Glass fibers.

The evolution in the change of the beam movements when subjected to an increasing electric field with the presence of several temperature differences is also studied, comparing the different responses for each temperature case. This analysis is shown in Figure 5.5.3 and Figure 5.5.4 in beams made of AS4/epoxy fibers.

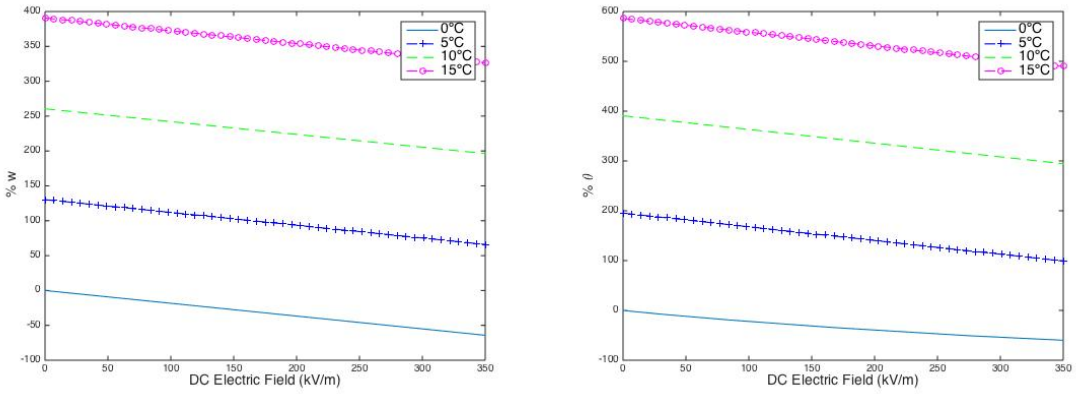

(a) Maximum change in vertical displacement (b) Maximum change in rotation

Figure 5.5.3: Sensitivity of maximum variation in a) vertical displacement and b) rotation to electric field for cantilever beams with AS4/epoxy fibers

	Vertical displacement	Rotation
Cantilever beam. AS4/epoxy fiber	-0.1834	-0.2445
Cantilever beam. E-Glass fiber	-0.1462	-0.1567
Simply supported beam. AS4/epoxy fiber	0.4413	0.5503
Simply supported beam. E-Glass fiber	0.2513	0.3134

Table 5.5.2: Different slopes for the vertical displacement and rotation variations versus electric field curves for a $[p_2/0_2/90_5]_{4S}$ cantilever and simply supported beam with AS4/epoxy or E-Glass fibers.

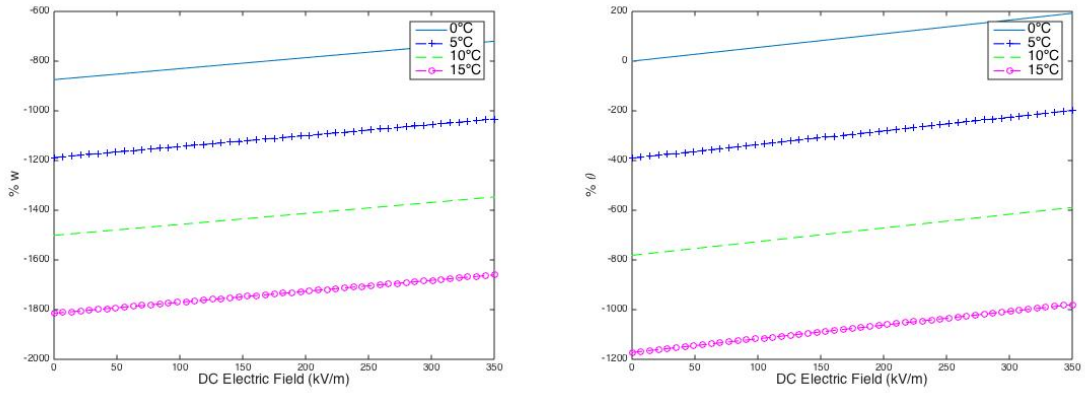

(a) (b)

Figure 5.5.4: Sensitivity of maximum variation in a) vertical displacement and b) rotation to electric field for simply supported beams

Although the same behaviors as in the previous temperature analyses are obtained, which is an enlargement of deformations for simply supported beams and a decrease in cantilever beams due to the respective addition and cancellation of both positive temperature and voltage gradient contributions. The relation of the changes in beam movements with the electric field remains linear. Beams made of E-Glass fibers exhibit the same behavior for the temperature difference sensitivity as the ones shown in Figures 5.5.1 and 5.5.2 for AS4/epoxy fibers but with different magnitudes. The corresponding slopes of these relations are expressed in Table 5.5.2.

CHAPTER 6

Conclusions and further studies

6.1 Summary and conclusions

The control capacity over the deflections produced in a structure with a piezoelectric material embedded has been studied in this Undergraduate Thesis Project. The control of movements of smart materials generates structures capable of changing its shape, which is applicable to the industry, enabling a real-time and optimum adaption to the operating requirements and a an improvement in the structure performance.

The piezoelectric capacity to control the beam deformations have been determined by assessing a sandwich beam with PZT introduced within its stacking sequence, exposed to a variable electric field in two different beam boundary conditions. The Classical Laminated Plate Theory have been modified to be applicable to a sandwich beam, accounting for the effect produced by the electric field. The effect produced by the presence of a temperature difference in the thickness direction is also introduced in the analysis.

Among the boundary conditions studied, simply supported beams have been found to enable higher variations in the beam deformations when compared to cantilever beams since the simply supported condition implies lower beam movements, so that the change in beam deformation produced by the electric field is referred to a lower value.

Furthermore, a dissimilarity in the direction of the beam response has been obtained for each boundary condition when exposed to either an electric field or a temperature difference relative to the null electric field state, which is caused by the difference in the theoretical boundary condition constants. One of the boundary constants of the simply supported movement description depends on the electric field and the temperature difference, while none of the boundary constants of the clamped case depend on them.

On one hand, a decrease in the beam vertical displacement and rotation is achieved in cantilever beams when they are subjected to a positive electric field. This effect is enhanced when there is a temperature difference along the beam

thickness with higher temperature at the bottom. On the other hand, for simply supported beams the opposite conditions are desired in order to decrease the beam deformations: a negative electric field presence and higher temperature at the top laminate than at the bottom ones.

Regarding the stacking sequence selection, the laminae order has been found to highly affect the capacity of control over the beam movements. When there is a presence of an electric field, piezoelectric material layers must be placed at the top of the laminate sequence in order to achieve the highest control variation as possible. This is because the greater distance from the piezoelectric material to the beam symmetry axis, the higher control capability it has over the beam deformations.

This distance to the symmetry axis can be augmented by increasing the core thickness of the sandwich beam. However the relation between the core thickness and the beam movement is parabolic, so that special care has to be taken in the core thickness versus movement control capacity tradeoffs, specially in those application of smart structures where weight is important, since the core thickness has a direct impact on it.

Nevertheless, those beams with the most suitable stacking sequence for the movement control by piezoelectricity, with the piezoelectric material placed at the top of the laminate, have exhibited less variation in the beam deflections when they are exposed to a temperature difference than other stacking sequences.

Therefore the capacity to modify the simple beam displacements have been proven to be achievable, quantifying some parameters that affect the tune capability effectiveness. However, the beam operating conditions highly influence the piezoelectric beam performance, so that they have to be deeply analyzed together with the structure functional requirements in order to determine the adequate structure characteristics, based on the conclusions achieved.

6.2 Future studies

This Undergraduate Thesis Project can be deepen by analyzing the effect of using laminae with fibers placed at +45°/-45° on the variation of beam deflections produced by the piezoelectric material. In addition, the theoretical analysis performed regarding the static beam movements can be extended and compared to the study of the piezoelectric capacity over the control of dynamic beam movements and vibrations.

Regarding the validation of the static analyses accomplished in this dissertation, a Finite Element Method (*FEM*) beam model capable of predicting the piezoelectric contribution should be modeled to compare the results obtained with the theoretical ones shown in this dissertation. FEMs would also have to be

used to validate dynamic movements and vibrations.

Smart materials possess verified benefits which have been assessed by progressive investigations on them. These studies have allow researchers to be aware that their implantation on industrial structures will result in either an increase in the structure performance or a reduction in the manufacturing or operating costs. Therefore their use will be more and more extended in future decades.

However the technological knowledge of smart materials has to be reinforced and widened to develop appropriate standards and regulations to deal with their characteristics. In addition, some of the drawbacks of smart materials must be overcome. For instance, PZT materials are desired to be replaced by other material with similar performance, since it contains high percentage of lead, which is a very toxic substance and therefore it is not allowed in some applications such as biological ones, so that its used is restricted in most of the countries.

Bibliography

[1] Ahmad,I., Smart Structures and Materials, Proceedings of U.S. Army Research Office Workshop on Smart Materials, Structures and Mathematical Issues, Virginia Polytechnic Institute & State University. *Technomic Publishing Co. (1988)*: 13-16.

[2] Gardiner,P.T., Smart structures and materials systems, In IFAC Symposia Series. *Oxford (1993)*: 127-135.

[3] Choi,S. and Han,Y., Piezoelectric Actuators: Control Applications of Smart Materials. *CRC Press (2010)*: 1-7.

[4] Kamila,S., Introduction, classification and applications of smart materials: an overview. *American Journal of Applied Sciences, 10. Science Publication (2013)*: 876-880.

[5] Gilewski,W. and Sabouni-Zawadzka,A., On possible applications of smart structures controlled by self-stress. *Archives of Civil and Mechanical Engineering,* ***15*** *(2015)*: 469-478.

[6] Rogers,C.A., Smart Material Systems and Structures, Proceedings of U.S.-Japan Workshop on Smart/Smart Materials and Systems, *Technomic Publishing Co., Inc. 1990)*: 11-33.

[7] Fairweather,J.A., Designing with Active Materials: An Impedance Based Approach. *UMI 1998)*: 196.

[8] Donald,J.L., Engineering Analysis of Smart Material Systems. *Wiley InterScience (2007).*

[9] Mäkelä,K.K., Characterization and performance of electrorheological fluids based on pine oils. *VTT Manufacturing Technology (1999).*

[10] Wen,W., Huang,X., Yang,S., Lu,K. and Sheng,P., The giant electrorheological effect in suspensions of nanoparticles. *Nature Materials* ***2*** *(2003)*: 727–730.

[11] Wen,W., Huang, X. and Sheng,P., Electrorheological fluids: Structure and mechanisms *Soft Matter,* ***4*** *(2008)*: 200-210.

[12] Wen,W. and Sheng,P.,Electrorheological Fluids: Mechanisms, Dynamics, and Microfluidics Applications. *Annual Review of Fluid Mechanics,* ***44*** *(2012)*: 143-174.

[13] Hao,T., Electrorheological Fluids: The Non-aqueous Suspensions. *Studies in Interface Science, **22** (2011)*: 518-553.

[14] Dutta,S. and Chakraborty,G., Modeling and characterization of a magneto-rheological fluid based damper and analysis of vibration isolation with the damper operating in passive mode. *Journal of Sound and Vibration, **353** (2015)*: 96–118.

[15] Kordonski,W. and Golini,D., Magnetorheological suspension-based high precision finishing technology (MRF). *J Intell Mater Syst Struct, **9** (1998)*: 650–654.

[16] Joule,J.P., On a new class of magnetic forces. *Annals of Electricity, Magnetism, and Chemistry, **8** (1842)*: 219–224.

[17] Olabi,A.G. and Grunwald,A., Design and Application of Magnetostrictive (MS) Materials. *Sensors and Actuators A., **144** (2008)*: 161–175.

[18] Calkins,F.T. and Flatau,A.B., Terfenol-D Sensor design and optimization. *Iowa State University.*

[19] Otsuka,K. and Wayman,C.M., Shape Memory Materials Cambridge University Press (1999): 1-49.

[20] Lagoudas,D., Shape Memory Alloys: Modeling and Engineering Applications *Chemistry and Materials Science, Springer (2008)*: 1-15.

[21] Ölander,A., An electrochemical investigation of solid cadmium-gold alloys. *Journal of the American Chemical Society **54** (1932)*: 3819–3833.

[22] Buehler,W.J., Gilfrich,J.W. and Wiley,R.C., Effects of Low-Temperature Phase Changes on the Mechanical Properties of Alloys Near Composition TiNi. *Journal of Applied Physics 34, **5** (1963)*: 1475–1477.

[23] Otsukaa,K. and Renb,X., Physical metallurgy of Ti–Ni-based shape memory alloys. *Progress in materials science, **50** (2005)*: 511-678.

[24] Miyazaki,S. and Mizukoshi,K., et al., 1999. Fatigue life of Ti-50 at% Ni and Ti–40Ni–10 Cu (at%) shape memory alloy wires. *Materials Science and Engineering A, **273–275** (1999)*: 658–663.

[25] Chopra,I. and Sirohi,J., Smart Structures Theory. *Cambridge Aerospace Series, **35** (2013)*: 194-305.

[26] Hill,K.O., Fujii,Y., Johnson,D.C. and Kawasaki,B.S., Photosensitivity in optical fiber waveguides: application to reflection fiber fabrication. *Appl. Phys. Lett. **32** (1978)*: 647.

[27] Cusano,A., Cutolo,A. and Albert,J., Fiber Bragg Grating Sensors: Recent Advancements, Industrial Applications and Market Exploitation. *Bentham Science Publishers (2011)*: 1-35.

[28] Miller,J.W. and Méndez,A., Fiber Bragg grating sensors: Market overview and new perspectives. *Fiber Bragg Grating Sensors: Recent Advancements, Industrial Applications and Market Exploitation. Bentham Science Publishers Ltd. (2011)*: 313-320.

[29] López,O., Carnicero,A. and Ruiz,R., Materiales inteligentes (II): Aplicaciones tecnológicas. *Anales de mecánica y electricidad, (January-February 2004).*

[30] Dufault,F. and Akhras,G., Smart Structure applications in aircraft. *The Canadian Air Force Journal (Summer 2008).*

[31] Leng,J., Asundia,A., Structural health monitoring of smart composite materials by using EFPI and FBG sensors. *Sensors and Actuators A: Physical* ***103*** *(2003)*: 330-340.

[32] Trojanowski,R. and Wiciak,J., Structural noise reduction and its effects on plate vibrations. *Acta Physica Polonica. A,* ***121*** *(2012).*

[33] Calkins,F.T., Boeing's Morphing Aerostructures. *Boeing Commercial Airplanes Enabling Technology and Research.*

[34] Abdullah,E.J., Simon Watkins,S., Application of smart materials for adaptiveairfoil control. *47th AIAA Aerospace Sciences Meeting Including the New Horizons Forum and Aerospace Exposition* (2009).

[35] Mabe,J.H., Calkins,F.T. and Butler,G.W., Boeing's Variable Geometry Chevron: Morphing aerostructure for jet noise reduction, *47nd AIAA Adaptive Structures Conference (2006).*

[36] Banke,J., NASA Helps Create a More Silent Night. NASA Aeronautics Research Mission Directorate (2010).

[37] Chen,Y., Sun,J., Liu,Y. and Leng,J., Variable stiffness property study on shape memory polymer composite tube. *Smart Material and Structures,* ***21*** *(2012).*

[38] Long,J., Hale,M., Mchenry,M. and Westneat,M., Functions of fish skin: flexural stiffness and steady swimming of long nose gar lepisosteus osseus. *J. Exp. Biol., 199 (1996)*: 2139–2151.

[39] Andersen,G.R., Cowan,D.L. and Piatak,D.J., Aeroelastic modeling, analysis and testing of a morphing wing structure. *Proc 48th AIAA/ASME/ASCE/AHS/ASC Structures, Structural Dynamics, and Materials Conf (2007).*

[40] Thill,C., Etches,J., Bond.I., Potter,K. and Weaver,P., Composite corrugated structures for morphing wing skin applications. *Smart Material and Structures,* ***19*** *(2010).*

[41] Lan, X.,Liu,Y., Lv,H., Wang,X., Leng,J. and Du,S., Fiber reinforced shape-memory polymer composite and its application in a deployable hinge. *Smart Material and Structures,* ***18*** *(2009).*

[42] Curie,J. and Curie,P., Development, via compression, of electric polarization in hemihedral crystals with inclined faces. *Bulletin de la Societe de Minerologique de France,* ***3*** *(1880)*: 90-93.

[43] Ballato,A., "Piezoelectricity: History and New Thrusts". *IEEE Ultrasonics Symposium,* ***1*** *(1996)*: 575-583.

[44] Voigt,W., Lehrbuch der Kristallphysik.

[45] Valasek,J., Piezoelectric and allied phenomena in Rochelle salt *Physical Review,* ***15*** *(1920).*

[46] Srinivasan,A.V. and McFarland,M., Smart Structures: Analysis and Design *Cambridge University Press (2001)*: 7-20.

[47] Dineva,P., Gross,D., Müller,R. and Rangelov,T., Dynamic fracture of piezoelectric materials. Solution of Time-Harmonic problems via BIEM. *Solid Mechanics and Its Applications,* ***12*** *(2014,)*: 7-12.

[48] Sreenivasa,S. and Arockiarajan A., Effective electromechanical response of macro-fiber composite (MFC): Analytical and numerical models. *International Journal of Mechanical Sciences,* ***77*** *(2013)*: 98–106.

[49] Newnham,R.E., Skinner,D.P. and Cross,L.E., Connectivity and piezoelectric-pyroelectric composites. *Materials Research Bulletin,* ***13****, 1978)*: 525–536.

[50] Meyer,J.L., Harrington,W.B., Agrawal,B.N. and Song,G., Vibration suppression of a spacecraft flexible appendage using smart material. *Smart Material and Structures,* ***7*** *(1998)*: 95–104.

[51] Kauffman,J.L. and Lesieutrey,G., Vibration Reduction of Turbomachinery Bladed Disks with Changing Dynamics using Piezoelectric Materials. *52nd AIAA/ASME/ASCE/AHS/ASC Structures, Structural Dynamics and Materials Conference (2011).*

[52] Sensor Technology Ltd. Active Noise and Vibration Control. *Smart Structures,* ***98-001*** *(1998).*

[53] Alaimoa,A., Milazzob,A. and Orlandoa,C., Numerical analysis of a piezoelectric structural health monitoring system for composite flange-skin delamination detection. *Composite Structures,* ***100*** *(2013)*: 343–355.

[54] Eugster,S., Geometric Continuum Mechanics and Induced Beam Theories. *Lecture Notes in Applied and Computational Mechanics,* ***75*** *(2015)*: 83-99.

[55] Reddy,J.N., Mechanics of laminated composite plates and shells: Theory and analysis. *CRC Press (2003)*: 113-175.

[56] Soden,P.D., Hinton,M.J. and Kaddour,A.S., Lamina properties, lay-up configurations and loading conditions for a range of fibre-reinforced composite laminae. *Composite Science and Technology (1998)*: 1011-1022.

[57] Pacheco,M., Mendoza,F., Santoyo, Méndez,A. and Zenteno,L.A., Piezoelectric-modulated optical fibre Bragg grating high-voltage sensor, Number 9. *Measurement Science and Technology,* ***10*** *(1999).*

[58] URL-1: CTS Electronic Components
`http://www.ctscorp.com/components/pzt/downloads/PZT_5Aand5H.pdf`

Appendix

Cost analysis

On this section, an estimation of the total cost of this dissertation is assessed. Total cost is defined as an addition of the equipment amortization and direct and indirect labor costs.

Equipment amortization costs:

Description	Amortization	Unitary cost	Total cost
Computer (HP Z400)	10%	700€	70€
MATLAB®	5%	2000€	100€

Table A.1: Equipment amortization costs.

Direct labor costs:

Description	Dedicated hours	Cost/hour	Total cost
Junior engineer	400	12€	4800€
Senior engineer	15	30€	450€

Table A.2: Direct labor costs.

Indirect labor costs:

Description	Dedicated hours	Cost/kWh	Computer energy consumption	Total cost
Electricity	400	0.144€	312 kW	14.23€

Table A.3: Indirect labor costs.

With these data, the total estimated cost of this Undergraduate Thesis Project is 5434.23€.